Low-energy photon scattering experiments of ^{151,153}Eu, ^{163}Dy, and ^{165}Ho and the systematics of the $M1$ scissors mode in odd-mass rare-earth nuclei

A. Nord,[1,*] J. Enders,[2] A. E. de Almeida Pinto,[3] D. Belic,[1,*] P. von Brentano,[4] C. Fransen,[4] U. Kneissl,[1] C. Kohstall,[1] A. Linnemann,[4] P. von Neumann-Cosel,[5] N. Pietralla,[4] H. H. Pitz,[1] A. Richter,[5] F. Stedile,[1] and V. Werner[4]

[1]*Institut für Strahlenphysik, Universität Stuttgart, D-70569 Stuttgart, Germany*

[2]*National Superconducting Cyclotron Laboratory, Michigan State University, East Lansing, Michigan 48824*

[3]*Instituto de Fisica, Universidade de São Paulo, 01489-970 São Paulo, Brazil*

[4]*Institut für Kernphysik, Universität zu Köln, D-50937 Köln, Germany*

[5]*Institut für Kernphysik, Technische Universität Darmstadt, D-64289 Darmstadt, Germany*

(Received 10 October 2002; published 18 March 2003)

Nuclear resonance fluorescence experiments were performed on the rare-earth nuclei ^{151,153}Eu, and with considerably increased sensitivity on ^{163}Dy and ^{165}Ho to study the fragmentation of the $M1$ scissors mode in odd-mass nuclei, and to clarify the puzzle of the missing total $M1$ strength observed for odd-mass nuclei so far. Using the bremsstrahlung photon beam of the Stuttgart Dynamitron (end point energy 4.05 MeV) and high-resolution Ge γ-ray spectrometers, detailed information was obtained on excitation energies, decay widths, transition probabilities, and branching ratios. Whereas in ^{151}Eu only 11 weak excitations were observed, 161 and 138 excitations could be detected in the heavier nuclei ^{163}Dy and ^{165}Ho, respectively. The results are compared to those observed recently at the Stuttgart facility for the neighboring odd-mass nuclei ^{161}Dy, ^{155,157}Gd, and ^{159}Tb. The measured total strengths increase with the mass number A. Ascribing the same portion of the dipole strength to $M1$ excitations as measured in the neighboring even-even nuclei, the total $M1$ strength deduced from the most sensitive experiment on ^{163}Dy is comparable to those found in the neighboring even-even nuclei. The results for ^{163}Dy and ^{165}Ho are compared with a fluctuation analysis of the photon scattering spectra to estimate the amount of still unresolved strength eventually hidden in the background due to the extreme fragmentation of the $M1$ scissors mode in odd-mass rare-earth nuclei. For ^{165}Ho, the total derived strength of $B(M1)\uparrow = 2.9(5)\mu_N^2$ agrees within error bars with an earlier analysis of a different measurement of the ^{165}Ho(γ,γ') reaction. In ^{163}Dy the method leads to an unphysical background shape, underlining the experimental observation of a significantly reduced fragmentation pattern of the dipole modes in this nucleus, which must be traced back to structure features of the Dy isotopes.

DOI: 10.1103/PhysRevC.67.034307 PACS number(s): 25.20.Dc, 21.10.Re, 23.20.Lv, 27.70.+q

I. MOTIVATION

Since its experimental discovery [1] almost two decades ago, the magnetic dipole scissors mode has been one of the most intensively studied problems of low-energy nuclear structure. A coherent picture starts to emerge for even-mass nuclei [2], in particular based on a comprehensive set of experimental data on rare-earth nuclei obtained with the high-resolution nuclear resonance fluorescence (NRF) technique [3]. The systematics of gross properties such as the mean energy and total $M1$ strength exhibit a close link to deformation properties which can be reproduced in sum-rule approaches [4–6] and with empirical parametrizations [7]. Microscopic descriptions are quite successful in reproducing the scissors mode strength distributions and their fragmentation (see, e.g. Refs. [8,9] and references therein), although some open questions remain.

The situation in odd-mass nuclei is more complicated. The first discovery of the scissors mode in ^{163}Dy [10] and subsequent experiments found significantly lower total strengths (with the exception of Ref. [11]), which would be hard to understand in the light of the findings discussed above. A solution to the problem was offered in Ref. [12] where it was demonstrated that because of the high level densities in odd-mass deformed nuclei, even high-resolution Ge γ-ray spectroscopy may not be sufficient to resolve all final states. Therefore, a part of the scissors mode strength is hidden unresolved in the experimental nonresonant background of the NRF spectra. With a fluctuation analysis technique [13,14], this part of the strength can be recovered. Then, the total scissors mode strengths are comparable to those in neighboring even-mass nuclei and consistent with the sum-rule predictions. However, some of the basic assumptions about the statistical properties of dipole strength distributions underlying the fluctuation analysis need to be reconsidered in view of a recent analysis of even-mass nuclei [15].

The present work contributes to various aspects of an improved understanding of the scissors mode properties in odd-mass rare-earth nuclei. New data are presented for the moderately deformed nuclei ^{151,153}Eu, thereby extending the experimental systematics towards the $N=82$ shell closure. The nucleus ^{165}Ho, which has been previously investigated at the S-DALINAC accelerator in Darmstadt [14], is measured with improved sensitivity and at a different end point energy. This dataset provides an important test case for the

*Present address: Agilent Technologies, D-71034 Böblingen, Germany.

fluctuation analysis technique and the underlying statistical assumptions. The analysis of the present data also allows one to investigate the consistency of the method, i.e., whether similar input parameters lead to a total dipole strength comparable to that of the previous result. Finally, a new measurement of ^{163}Dy with much improved sensitivity compared to the earlier data [10] was performed, because this nucleus showed an unusual strength distribution with much less fragmentation than any other case. The new results demonstrate how much of the strength was missed previously due to the experimental detection limit, and provide a further test case for the fluctuation analysis technique whose applicability to the odd-mass Dy isotopes remained unclear [12].

II. EXPERIMENTAL TECHNIQUES

A. Nuclear resonance fluorescence

The NRF, scattering of real photons off bound states, has proved to be the most sensitive tool for the investigation of low-lying dipole excitations in heavy nuclei [3]. The use of a photon source of a continuous energy distribution, such as bremsstrahlung, allows the simultaneous excitation of all levels with a sufficiently large ground-state transition width Γ_0. The total elastic scattering cross section I_S, energy integrated over a single resonance and integrated over the full solid angle equals

$$I_S = g\left(\frac{\pi\hbar c}{E_x}\right)^2 \frac{\Gamma_0^2}{\Gamma}, \tag{1}$$

with Γ the total decay width and g a statistical factor depending on the ground-state spin J_0 and the spin J of the excited level:

$$g = \frac{2J+1}{2J_0+1}. \tag{2}$$

From the measured total cross section I_S, the product $g\Gamma_0^2/\Gamma$ can be determined, see Eq. (1). The reduced dipole excitation probabilities $B(E1)\uparrow$ or $B(M1)\uparrow$ are directly connected to the product $g\Gamma_0$,

$$B(E1)\uparrow = 0.955\left(\frac{g\Gamma_0}{E_x^3}\right)(10^{-3}e^2\,\mathrm{fm}^2), \tag{3}$$

$$B(M1)\uparrow = 0.0864\left(\frac{g\Gamma_0}{E_x^3}\right)(\mu_N^2), \tag{4}$$

with the transition width Γ_0 in meV and the excitation energy E_x in MeV. Therefore, the dipole excitation probabilities can be derived from the measured scattering cross sections I_S for known branching ratios Γ_0/Γ, even without knowledge of the spins J of the excited states and the statistical factors g. The formalism describing NRF experiments is summarized in more detail in previous review papers [3,16].

Unfortunately, in the case of odd-mass target nuclei, one has to deal with certain principal drawbacks. The angular distributions of the scattered photons are rather isotropic. Therefore, in general no unambiguous spin assignments to the photoexcited states are possible, as for even-even nuclei, in particular not for isotopes with large ground-state spins like ^{151,153}Eu ($J_0^\pi = 5/2^+$), ^{163}Dy ($J_0^\pi = 5/2^-$), and ^{165}Ho ($J_0^\pi = 7/2^-$). Furthermore, no parity assignments are possible by linear polarization measurements as in the favorable case of even-even nuclei [3], since the nearly vanishing anisotropy in the angular distributions leads to rather low degrees of polarization of the scattered photons.

For the comparison of the strengths observed in odd-mass isotopes with those in even-even nuclei, the quantity $g\Gamma_0^{red}$ is introduced,

$$g\Gamma_0^{red} = g\frac{\Gamma_0}{E_x^3}, \tag{5}$$

which is proportional to the reduced dipole excitation probabilities, see Eqs. (3) and (4). In some favorable cases, information on the spins J of the photoexcited states can be extracted from the measured decay branching ratio R_{expt} to lower-lying states. This quantity R_{expt} is defined as

$$R_{expt} = \frac{B(\Pi L; J\rightarrow J_f)}{B(\Pi L; J\rightarrow J_0)} = \frac{\Gamma_f}{\Gamma_0}\left(\frac{E_{\gamma J_0}^3}{E_{\gamma J_f}^3}\right). \tag{6}$$

For deformed nuclei, in the rotational limit, the branching ratio R_{theo} can be calculated analytically

$$R_{theo} = \left|\frac{\sqrt{2J_f+1}\langle J_f,K_f,L,K-K_f|J,K\rangle}{\sqrt{2J_0+1}\ \langle J_0,K_0,L,K-K_0|J,K\rangle}\right|^2, \tag{7}$$

and allows the K quantum number of the excited state to be determined assuming the validity of these so-called Alaga rules [17].

Besides these physical drawbacks in principle, another more experimental problem arises in photon scattering experiments in the case of odd-mass nuclei. It is related to the strong fragmentation of dipole strength. The effect of the much smaller cross sections observed for excitations in odd-mass nuclei as compared to the even-even nuclei is twofold. First, since the background from nonresonant scattering of the incident bremsstrahlung beam remains the same as in even-even nuclei, the NRF measurements on odd-mass nuclei require a much higher experimental sensitivity. Furthermore, even small amounts of impurities ($\leqslant 2\%$) of the neighboring even-even isotopes give rise to peaks in the photon scattering spectra, comparable in size to the strongest peaks for excitations in the odd-mass isotopes (see, e.g., Refs. [18,19]). This demonstrates the necessity of targets with the highest available enrichment. Furthermore, the excitations in the neighboring even-even isotopes have to be well known, to avoid wrong assignments.

B. Experimental setup and details

The experiments were performed at the bremsstrahlung facility of the Stuttgart Dynamitron accelerator [3,18]. The end point energy of the bremsstrahlung beam was 4.05 MeV

TABLE I. Beam parameters and measuring times.

Isotope	End point energy (MeV)	Electron current (μA)	Measuring time (h)
^{151}Eu	4.05	260	130
^{153}Eu	4.05	220	120
^{163}Dy	4.05	260	460
^{165}Ho	4.05	250	110
^{165}Ho	4.05	250	40

in all experiments. The dc electron currents used in the present experiments had to be limited to about 250 μA corresponding to a maximum beam power of 1 kW, due to the thermal capacity of the radiator target. The beam parameters and total effective times of data collection are summarized in Table I. The compositions, total masses, and major impurities of the enriched scattering targets are given in Table II. These NRF targets were sandwiched by ^{27}Al disks (diameter 16 mm), serving for the photon flux calibration [20]. Their total masses are also given in Table II.

The scattered photons were detected by three high-resolution Ge γ-ray spectrometers installed at angles of about 90°, 127°, and 150° with respect to the incoming bremsstrahlung beam. In the first experiments on ^{151,153}Eu and ^{165}Ho, the two detectors under 90° and 127° had an efficiency of about 100%, relative to a standard 7.6 $\times$7.6 cm^2 NaI(Tl) detector, while the additional detector under 150° had a relative efficiency of 20%. The energy resolutions were typically about 2 keV at a photon energy of 1.3 MeV, and about 3 keV at 3 MeV. In the most sensitive experiments on ^{163}Dy, three 100% efficiency detectors were available and the detector at 127° was surrounded additionally by a BGO anti-Compton shield.

To realize a narrow detector geometry, a special fourfold modular BGO setup [21] was used. With this arrangement the peak-to-background ratio could be improved by a factor of about 2. Furthermore, single- and double-escape peaks are strongly suppressed by using the BGO shield [22], facilitating together with the good energy resolution of the detectors considerably the analysis of the complex photon spectra with a huge number of densely spaced, partially overlapping lines. The detection limits achieved in the experiments on ^{165}Ho and ^{163}Dy are shown in Fig. 1. The detection limits are deduced by requiring the following criteria in the analysis to identify ''true'' peaks. The line contents had to be more than

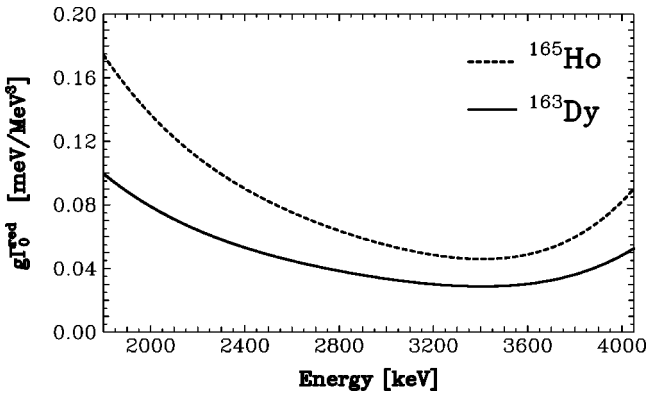

FIG. 1. Detection limits in the present photon scattering experiments on ^{165}Ho (dashed line) and ^{163}Dy (solid line). Plotted are the minimal reduced ground-state transition width Γ_0^{red} times the spin factor g as a function of the excitation energy, needed for levels to be detected. The criteria are given in the text. [$g\Gamma_0^{red}$ = 0.01 meV/MeV^3 corresponds to $B(E1)\uparrow = 0.955\times10^{-5}\ e^2$ fm^2 or $B(M1)\uparrow = 0.864\times10^{-3}\ \mu_N^2$].

2 standard deviations σ above the corresponding continuous background; additionally, the lines had to be detected in at least two detectors and the linewidths had to be in agreement with the detector energy resolutions as measured in the calibration runs using a ^{56}Co γ-ray source. Plotted in Fig. 1 are the minimal reduced ground-state transition widths Γ_0^{red} times the spin factor g as a function of the excitation energy, needed for levels to be detected in the present experiments [a value of $g\Gamma_0^{red} = 0.01$ meV/MeV^3 corresponds to $B(E1)\uparrow = 0.955\times10^{-5}e^2$ fm^2 or $B(M1)\uparrow = 0.864\times10^{-3}\ \mu_N^2$]. The somewhat better detection limit achieved in the ^{163}Dy experiments is mainly due to the availability of the BGO shield and the increased running time of 460 h. The total sensitivity in the present ^{163}Dy experiments could be improved by a factor of about 20 as compared to our previous experiments on ^{163}Dy, where scissors mode excitations could be detected for the first time in an odd-mass nucleus [10]. It should be emphasized that in the present experiments on ^{163}Dy an excellent detection limit could be achieved in the energy range of the scissors mode of about $3\times10^{-3}\ \mu_N^2$, by far the best value obtained in low-energy photon scattering experiments off heavy nuclei using bremsstrahlung beams [3].

Since no coincidence experiments are feasible at present NRF setups, possible decays of the photoexcited states to low-lying excited states (inelastic transitions) were searched

TABLE II. Target compositions and specifications.

Isotope	Composition	Enrichment (%)	Total masses (mg)		Major impurities
			Target	^{27}Al	
^{151}Eu	Eu_2O_3	99.24	2161	781	^{153}Eu (0.76%)
^{153}Eu	Eu_2O_3	99.81	1729	1016	^{151}Eu (0.19%)
^{163}Dy	Dy_2O_3	89.90	2530	506	^{161}Dy (0.26%); ^{162}Dy (1.82%); ^{164}Dy (8.02%)
^{165}Ho	Ho_2O_3	100	2697	763	
^{165}Ho	Ho metal	100	2315		

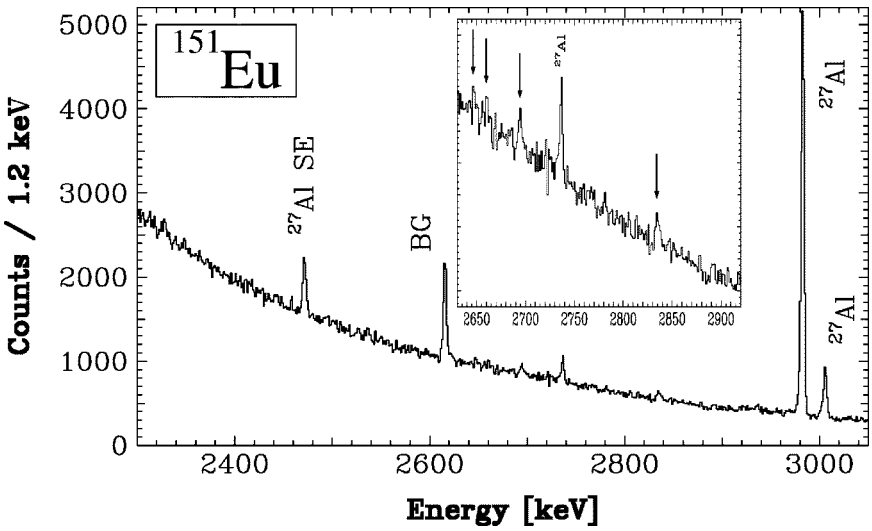

FIG. 2. Spectrum of photons scattered off ^{151}Eu in the energy range 2.3–3.3 MeV. All stronger, labeled peaks stem from the photon flux standard ^{27}Al, or from background (BG, ^{208}Pb). The inset shows with an expanded scale that part of the spectrum where most of the identified peaks, marked by arrows, occur.

for by applying the Ritz combination rule:

$$E_i-(E_x-E_f)\leqslant|\Delta E|, \tag{8}$$

with E_x, E_i, and E_f the level excitation energy, the energy of a possibly inelastic transition, and the energy of the final low-lying excited state (first or second excited state). For the assignments of inelastic transitions, a limit of $\Delta E = \pm 1$ keV was chosen, which corresponds to a realistic value of the total uncertainties in the needed energy determinations. Possible transitions to higher-lying excited states were neglected.

III. EXPERIMENTAL RESULTS

The strong fragmentation of the dipole strength in the investigated odd-mass nuclei leads to an increased level density and reduced strengths of the individual lines. On the other hand, the continuous background from nonresonant scattering is the same as for the neighboring even-even nuclei. Therefore, the observed spectra are rather complex and exhibit a worse peak-to-background ratio as compared to the spectra for even-even nuclei. The uncertainties of the quoted excitation energies can be estimated conservatively to be smaller than $\Delta E_x \leqslant 1$ keV.

Since neither spins nor parities could be determined in the present NRF experiments, it was assumed that all levels are exclusively excited via pure dipole transitions. From the measured total scattering cross sections I_S, the quantities $g\Gamma_0^{red}$ were deduced assuming isotropic angular distributions of the scattered photons and taking into account observed decay branchings to lower-lying excited states (Γ_i/Γ_0; $i = 1,2,\ldots$). These values were converted into reduced excitation probabilities $B(M1)\uparrow$ assuming $M1$ excitations, the corresponding numbers are given in the tables of this section. If some of the excitations are of $E1$ character, the reduced excitation probabilities $B(M1)\uparrow$ can be easily translated into $B(E1)\uparrow$ values ($1\mu_N^2$ corresponds to $11.06\times10^{-3}e^2$ fm^2).

A. Results for ^{151}Eu(γ,γ')

A part of the spectrum of photons scattered off ^{151}Eu is depicted in Fig. 2. The spectrum is dominated by the ^{27}Al calibration lines and a known background peak (^{208}Pb) from natural environmental radiation. Furthermore, a small peak visible at 3089 keV can be attributed to ^{13}C, which is contained to only 1.1% in the carbon of the plastic envelope of the scattering target material. Only a few very small peaks could be detected above the continuous background from nonresonant scattering which increases exponentially towards lower energies. In total, 11 excitations could be observed in the investigated energy range up to 4 MeV. For all levels only transitions to the $J_o^\pi = 5/2^+$ ground state were observed.

The numerical results are summarized in Table III. Given are the excitation energies E_x, the total scattering cross sections I_S, the product of the statistical factor g times the ground-state widths Γ_0, respectively, the reduced ground-

TABLE III. Numerical results of the ^{151}Eu experiment: excitation energies E_x, the total scattering cross sections I_S, the product of the statistical factor g times the ground-state widths Γ_0, respectively, the reduced ground-state widths Γ_0^{red}, and the reduced excitation strengths $B(M1)\uparrow$, assuming only $M1$ excitations.

E_x (keV)	I_s (eV b)	$g\Gamma_0$ (meV)	$g\Gamma_0^{red}$ (meV/MeV^3)	$B(M1)\uparrow$ (μ_N^2)
889	3.80(63)	0.78(13)	1.11(18)	0.096(16)
1421	2.36(43)	1.24(22)	0.43(8)	0.037(7)
1803	1.29(26)	1.09(22)	0.19(4)	0.016(3)
2327	1.17(20)	1.65(29)	0.13(2)	0.011(2)
2535	0.91(18)	1.52(30)	0.09(2)	0.008(2)
2647	0.79(17)	1.45(32)	0.08(2)	0.007(2)
2659	0.89(17)	1.64(31)	0.09(2)	0.008(1)
2694	1.07(17)	2.02(32)	0.10(2)	0.009(1)
2834	1.17(16)	2.44(33)	0.11(2)	0.009(1)
3838	0.89(23)	3.41(90)	0.06(2)	0.005(1)
3918	1.18(29)	4.73(115)	0.08(2)	0.007(2)

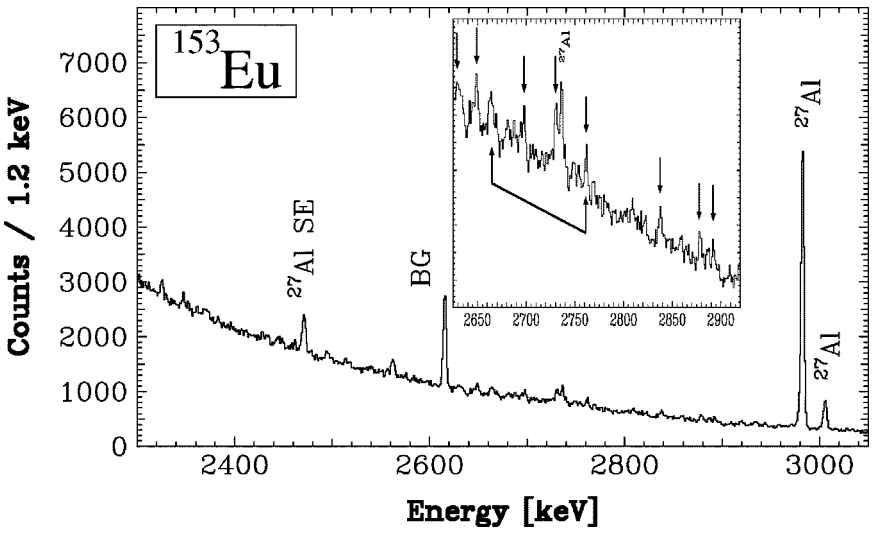

FIG. 3. Spectrum of photons scattered off ^{153}Eu in the energy range 2.3–3.3 MeV. All stronger, labeled peaks stem from the photon flux standard ^{27}Al, and from background (BG, ^{208}Pb). Some weaker lines are also visible belonging to excitations in ^{153}Eu. The inset shows with an expanded scale the part of the spectrum where most of the identified peaks, marked by arrows, occur. The bracket connects the elastic ground-state transition of the level at 2761 keV and the corresponding inelastic transition to the second excited state at 97.4 keV.

state widths Γ_0^{red}, and the reduced excitation strengths $B(M1)\uparrow$, assuming pure $M1$ excitations. The total detected excitation strength in the energy range from 2 to 4 MeV amounts to only $\Sigma_{2-4\ \mathrm{MeV}}\, g\Gamma_0^{red}=(0.95\pm0.19)$ meV/MeV^3 corresponding to $\Sigma_{2-4\ \mathrm{MeV}}\, B(M1)\uparrow=(0.082\pm0.017)\mu_N^2$, assuming exclusively $M1$ excitations.

B. Results for ^{153}Eu(γ,γ')

A part of the spectrum of photons scattered off ^{153}Eu is displayed in Fig. 3. As in the case of ^{151}Eu, the spectrum is also dominated by the ^{27}Al calibration lines and the known ^{208}Pb background peak. However, several weak peaks could clearly be detected, which can be ascribed to excitations in ^{153}Eu. In total 15 new levels could be observed in the investigated energy range up to 4 MeV. For 13 of these states, only transitions to the $J_0^\pi=5/2^+$ ground state could be observed. Their properties are summarized in numerical form in Table IV. In contrast to the ^{151}Eu experiments, in ^{153}Eu for two levels a decay branching to lower-lying excited states could be detected. For the level at 1177 keV, a decay to the second excited state at 83.9 keV within the ground-state rotational band was observed. For the state at 2761 keV, a branching to the $J^\pi=5/2^-$ bandhead could be detected. In Table V the numerical data for these two levels are summarized. In addition to the quantities quoted in the preceding tables, the branching ratios R_{expt}, the spins J of the photoexcited levels, and the spins J_f of the populated excited states are given.

The total detected excitation strength in the energy range from 2 to 4 MeV is remarkably higher than in ^{151}Eu, however, it is still about one order of magnitude smaller as the strengths observed in heavier midshell even-even rare-earth nuclei. For ^{153}Eu, it amounts to $\Sigma_{2-4\ \mathrm{MeV}}\, g\Gamma_0^{red}=(3.55\pm0.53)$ meV/MeV^3 corresponding to $\Sigma_{2-4\ \mathrm{MeV}}\, B(M1)\uparrow=(0.307\pm0.046)\mu_N^2$, assuming exclusively $M1$ excitations.

C. Results for ^{163}Dy(γ,γ')

Figure 4 shows a part of the spectrum of photons scattered off ^{163}Dy. It consists of numerous densely spaced peaks, some of them comparable in strength with the ^{208}Pb background and ^{27}Al calibration lines that dominated the ^{151,153}Eu spectra. In addition, near 2900 keV, and between 3000 and 3100 keV, bumps are visible, exceeding the exponentially decreasing continuous background. These broad structures are due to an extreme density of lines, which cannot be resolved completely. Merely, the knowledge of the linewidths from the calibration runs allows a reasonable analysis.

Another problem arises from the impurities of the available target material enriched to only 89.9% in ^{163}Dy (see Table II). From 44 transitions known in ^{164}Dy from our previous experiments [18,23], nearly all [41 transitions (besides only three weak transitions)] could be identified in the present measurements in spite of the fact that only 8% of the enriched ^{163}Dy target material consisted of ^{164}Dy. This shows on the one hand the sensitivity of the present measurements, and on the other hand it demonstrates the necessity of using extremely enriched targets and/or the need of a suffi-

TABLE IV. Numerical results of the ^{153}Eu experiment for levels for which only ground-state transitions could be detected. The quoted quantities are the same as in Table III.

E_x (keV)	I_s (eV b)	$g\Gamma_0$ (meV)	$g\Gamma_0^{red}$ (meV/MeV^3)	$B(M1)\uparrow$ (μ_N^2)
1156	3.70(68)	1.29(24)	0.83(15)	0.072(13)
2295	2.61(46)	3.58(63)	0.30(5)	0.026(5)
2324	2.97(45)	4.18(63)	0.33(5)	0.029(4)
2346	2.54(42)	3.64(60)	0.28(5)	0.024(4)
2369	2.10(41)	3.07(61)	0.23(5)	0.020(4)
2561	4.33(53)	7.39(91)	0.44(5)	0.038(5)
2630	1.75(34)	3.15(61)	0.17(3)	0.015(3)
2648	2.54(37)	4.64(68)	0.25(4)	0.022(3)
2697	2.11(37)	3.99(70)	0.20(4)	0.018(3)
2730	4.03(46)	7.81(90)	0.38(4)	0.033(4)
2837	1.95(34)	4.09(71)	0.18(3)	0.016(3)
2878	2.40(37)	5.18(80)	0.22(3)	0.019(3)
2891	0.77(18)	1.69(39)	0.07(2)	0.006(1)

TABLE V. Numerical results of the ^{153}Eu experiment for levels exhibiting a decay branching. Besides the quantities given in the preceding tables, the branching ratios R_{expt}, the spins J of the photoexcited levels, and the spins J_f of the fed lower-lying states ($7/2^+$: first excited state at 83.4 keV, $5/2^-$: second excited state at 97.4 keV) are given.

E_x (keV)	I_s (eV b)	$g\Gamma_0$ (meV)	R_{expt}	J_f^π	J	$g\Gamma_0^{red}$ (meV/MeV^3)	$B(M1)\uparrow$ (μ_N^2)
1177	27.48(188)	13.16(77)	0.41(5)	$7/2^+$	5/2	8.07 (47)	0.698 (41)
2761	2.59(38)	10.35(110)	1.13(24)	$5/2^-$		0.49 (5)	0.043 (5)

cient knowledge of all states in the neighboring stable, even-even isotopes when investigating odd-mass nuclei. Unfortunately, the 2212 keV line stemming from a calibration transition in ^{27}Al superimposes a 2213 keV peak from a transition in ^{163}Dy, as known from our previous investigation of ^{163}Dy [10] where also measurements without Al target disks were performed. With the known scattering cross section of this 2213 keV state and those for strong excitations at 2180 and 2958 keV, the overlapping peaks at 2213 keV (^{163}Dy) and 2212 keV (^{27}Al) could be disentangled properly.

In total, 161 levels could be observed in the investigated energy range up to 4 MeV, which can be ascribed to excitations in ^{163}Dy. The properties of all states for which only transitions to the $J_0^\pi = 5/2^-$ ground state could be observed are summarized in numerical form in Table VI. For 39 states, decay branchings to the first excited state ($J_f^\pi = 7/2^-$; $E_f = 73.4$ keV) and/or to the second excited state ($J_f^\pi = 9/2^-$; $E_f = 167.3$ keV) within the ground-state rotational band could be observed. The properties of these states are summarized in numerical form in Table VII.

Unfortunately, in several cases an unambiguous assignment of inelastic transitions is not possible with the Ritz combination principle. In view of the high level density, it may happen that a transition can be interpreted as a ground-state transition as well as an inelastic transition from a higher-lying, excited state. Furthermore, it occurred that peaks may come from an inelastic transition to the level at 73.4 keV or to the second excited state at 167.3 keV. In these questionable cases the possible assignment was preferred where the energy differences of elastic and inelastic transitions were closer to the exact values of 73.4 and 167.3 keV, respectively. These assignments are included in Table VII. Possible alternative interpretations as ground-state transitions and inelastic transitions are summarized in Table VIII. However, these unambiguities have, within the error bars of the present experiment, no significant influence on the summed strengths discussed below.

The total detected excitation strength in the energy range from 2 to 4 MeV is remarkably higher than in the ^{151,153}Eu isotopes. It amounts to $\Sigma_{2-4\ \mathrm{MeV}}\, g\Gamma_0^{red} = (38.2 \pm 4.2)$ meV/MeV^3 corresponding to $\Sigma_{2-4\ \mathrm{MeV}}\, B(M1)\uparrow = (3.30 \pm 0.36)\,\mu_N^2$, assuming exclusively $M1$ excitations.

D. Results for ^{165}Ho(γ,γ')

In Fig. 5, a part of the spectrum of photons scattered off ^{165}Ho is depicted. As in the case of ^{163}Dy, a large number of peaks is visible, some of them comparable in height with the ^{208}Pb background and ^{27}Al calibration lines. The analysis of the spectrum for ^{165}Ho was easier to some extent since ^{165}Ho is monoisotopic, i.e., no lines from target impurities can occur and spoil the spectra. Nevertheless, problems similar to the ones for the ^{163}Dy spectra arose. First, the width of the peak at 2982 keV and the ratio of its area to those of the other two ^{27}Al peaks at 2212 keV and 3957 keV clearly show that there is a random overlap of the strong 2982 keV ^{27}Al transition with a weaker transition in ^{165}Ho. For a cor-

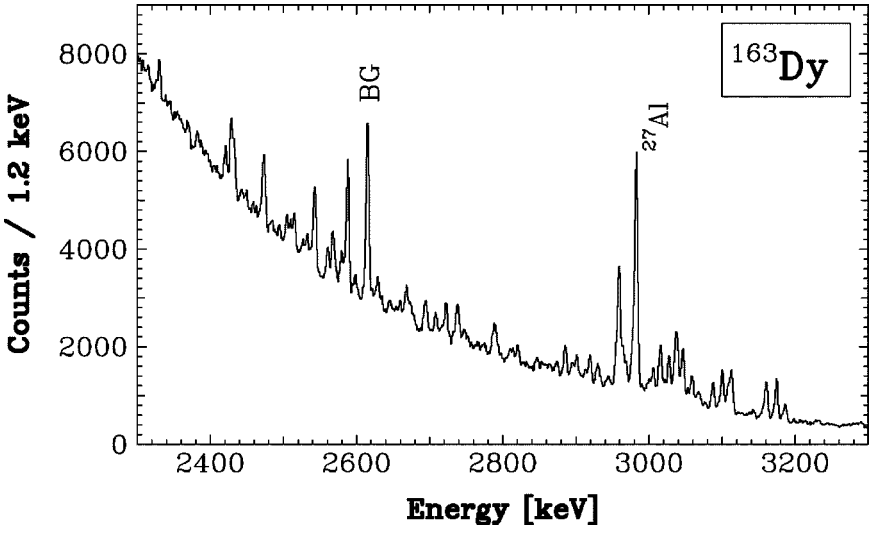

FIG. 4. Spectrum of photons scattered off ^{163}Dy in the energy range 2.3–3.3 MeV. Numerous partially strong peaks belong to excitations in ^{163}Dy (see text). The lines from the photon flux standard ^{27}Al and from background (BG, ^{208}Pb) are labeled.

TABLE VI. Numerical results of the ^{163}Dy experiment for levels for which only ground-state transitions could be detected. The quoted quantities are the same as in Table III.

E_x (keV)	I_s (eV b)	$g\Gamma_0$ (meV)	$g\Gamma_0^{red}$ (meV/MeV^3)	$B(M1)\uparrow$ (μ_N^2)
1542	1.62(27)	1.00(17)	0.27(5)	0.024 (4)
1684	1.04(22)	0.77(17)	0.16(4)	0.014 (3)
1705	1.31(24)	0.99(18)	0.20(4)	0.017(3)
1730	1.59(25)	1.24(19)	0.24(4)	0.021(3)
1775	3.20(35)	2.63(29)	0.47(5)	0.041(4)
1797	2.60(30)	2.18(26)	0.38(4)	0.033(4)
1831	1.00(21)	0.88(19)	0.14(3)	0.012(3)
1840	1.03(21)	0.91(19)	0.15(3)	0.013(3)
1902	1.36(22)	1.28(21)	0.19(3)	0.016(3)
1981	1.03(21)	1.05(22)	0.14(3)	0.012(2)
1984	0.75(20)	0.77(21)	0.10(3)	0.009 (2)
2009	1.29(22)	1.36(23)	0.17(3)	0.014 (3)
2054	1.03(19)	1.13(21)	0.13(2)	0.011 (2)
2080	1.17(20)	1.32(22)	0.15(3)	0.013 (2)
2091	0.99(19)	1.13(21)	0.12(2)	0.011 (2)
2099	0.84(20)	0.96(23)	0.10(3)	0.009 (2)
2112	0.70(18)	0.81(21)	0.09(2)	0.008 (2)
2158	0.81(17)	0.98(21)	0.10(2)	0.008 (2)
2165	1.19(21)	1.45(25)	0.14(3)	0.012 (2)
2169	1.22(21)	1.50(26)	0.15(3)	0.013 (2)
2224	0.98(18)	1.26(23)	0.12(2)	0.010 (2)
2237	0.93(20)	1.21(26)	0.11(2)	0.009 (2)
2255	1.07(22)	1.42(29)	0.12(3)	0.011 (2)
2272	0.98(18)	1.31(24)	0.11(2)	0.010 (2)
2278	1.54(20)	2.07(27)	0.18(2)	0.015 (2)
2287[a]	1.44(20)	1.97(28)	0.16(2)	0.014 (2)
2329	1.18(26)	1.66(37)	0.13(3)	0.011 (3)
2344	0.96(19)	1.37(28)	0.11(2)	0.009 (2)
2353	0.72(21)	1.04(30)	0.08(2)	0.007 (2)
2356	0.63(21)	0.91(30)	0.07(2)	0.006 (2)
2367	0.90(22)	1.31(33)	0.10(3)	0.009 (2)
2369	1.01(27)	1.48(39)	0.11(3)	0.010 (3)
2380	2.00(23)	2.95(34)	0.22(3)	0.019 (2)
2387	1.52(20)	2.25(30)	0.17(2)	0.014 (2)
2427	6.11(58)	9.37(90)	0.66(6)	0.057 (5)
2431	4.90(48)	7.54(73)	0.53(5)	0.045 (4)
2442[b]	0.88(17)	1.36(26)	0.09(2)	0.008 (2)
2449	0.95(16)	1.49(26)	0.10(2)	0.009 (2)
2473	6.14(57)	9.78(91)	0.65(6)	0.056 (5)
2483	1.10(17)	1.77(27)	0.12(2)	0.010 (2)
2503	1.29(18)	2.11(30)	0.13(2)	0.012 (2)
2527	1.14(18)	1.89(31)	0.12(2)	0.010 (2)
2542	8.74(85)	14.71(143)	0.90(9)	0.077 (8)
2559	3.60(35)	6.14(59)	0.37(4)	0.032 (3)
2567	5.40(51)	9.26(88)	0.55(5)	0.047 (5)
2570	1.55(23)	2.67(40)	0.16(2)	0.014 (2)
2627	3.69(35)	6.63(62)	0.37(3)	0.032 (3)
2658	2.26(24)	4.16(44)	0.22(2)	0.019 (2)
2666	3.20(34)	5.93(63)	0.31(3)	0.027 (3)
2669	1.71(28)	3.16(52)	0.17(3)	0.014 (2)
2698	0.71(16)	1.34(30)	0.07(2)	0.006 (1)

TABLE VI. (*Continued*).

E_x (keV)	I_s (eV b)	$g\Gamma_0$ (meV)	$g\Gamma_0^{red}$ (meV/MeV^3)	$B(M1)\uparrow$ (μ_N^2)
2715	1.29(20)	2.48(38)	0.12(2)	0.011 (2)
2724	0.61(20)	1.18(39)	0.06(2)	0.005 (2)
2752	0.94(15)	1.86(30)	0.09(1)	0.008 (1)
2765	0.70(14)	1.38(27)	0.07(1)	0.006 (1)
2774	1.12(22)	2.23(44)	0.11(2)	0.009 (2)
2790	2.02(26)	4.09(53)	0.19(2)	0.016 (2)
2808	1.52(20)	3.12(40)	0.14(2)	0.012 (2)
2830	0.64(13)	1.33(27)	0.06(1)	0.005 (1)
2847	1.22(24)	2.57(50)	0.11(2)	0.010 (2)
2853	1.04(18)	2.20(39)	0.10(2)	0.008 (1)
2859	0.82(23)	1.74(49)	0.07(2)	0.006 (2)
2873[b]	2.13(20)	4.58(44)	0.19(2)	0.017 (2)
2894	2.13(21)	4.65(46)	0.19(2)	0.017 (2)
2911	0.71(14)	1.56(31)	0.06(1)	0.006 (1)
2918[a]	4.15(33)	9.20(74)	0.37(3)	0.032 (3)
2928	2.47(28)	5.51(62)	0.22(3)	0.019 (2)
2931	1.35(21)	3.02(48)	0.12(2)	0.010 (2)
2942	1.07(17)	2.42(38)	0.10(2)	0.008 (1)
2963	6.99(53)	15.97(121)	0.61(5)	0.053 (4)
2968	4.16(34)	9.54(78)	0.37(3)	0.032 (3)
2976	4.69(38)	10.82(88)	0.41(3)	0.036 (3)
2988	0.86(14)	2.00(32)	0.08(1)	0.007 (1)
2997	1.50(17)	3.52(40)	0.13(2)	0.011 (1)
3026	7.13(65)	17.00(154)	0.61(6)	0.053 (5)
3034	7.34(72)	17.58(174)	0.63(6)	0.054 (5)
3037	8.07(79)	19.37(189)	0.69(7)	0.060 (6)
3045[b]	12.06(87)	29.10(211)	1.03(8)	0.089(6)
3052	1.89(18)	4.59(44)	0.16(2)	0.014 (1)
3057	5.31(40)	12.92(98)	0.45(3)	0.039 (3)
3067	2.97(24)	7.26(60)	0.25(2)	0.022 (2)
3087	1.25(19)	3.10(47)	0.11(2)	0.009 (1)
3099	6.83(51)	17.08(127)	0.57(4)	0.050 (4)
3107	4.63(36)	11.62(91)	0.39(3)	0.034 (3)
3125	0.50(11)	1.28(27)	0.04(1)	0.004 (1)
3137	0.67(15)	1.73(39)	0.06(1)	0.005 (1)
3142	2.07(19)	5.32(49)	0.17(2)	0.015 (1)
3173	1.92(21)	5.03(54)	0.16(2)	0.014 (2)
3186	3.67(34)	9.70(89)	0.30(3)	0.026 (2)
3206	0.53(12)	1.41(32)	0.04(1)	0.004 (1)
3264	0.49(11)	1.37(30)	0.04(1)	0.003 (1)
3282	0.69(16)	1.92(46)	0.05(1)	0.005 (1)
3301	0.41(11)	1.16(30)	0.03(1)	0.003 (1)
3390	0.58(11)	1.73(34)	0.05(1)	0.004 (1)
3404	0.46(11)	1.39(33)	0.04(1)	0.003 (1)
3416	1.30(15)	3.94(47)	0.10(1)	0.009 (1)
3423	0.54(11)	1.66(35)	0.04(1)	0.004 (1)
3434	0.64(15)	1.95(48)	0.05(1)	0.004 (1)
3449[b]	1.22(15)	3.78(46)	0.09(1)	0.008 (1)
3459	0.79(14)	2.46(42)	0.06(1)	0.005 (1)
3495	0.82(15)	2.61(47)	0.06(1)	0.005 (1)
3500	0.66(14)	2.09(46)	0.05(1)	0.004 (1)
3508	0.96(30)	3.09(96)	0.07(2)	0.006 (2)

TABLE VI. (*Continued*).

E_x (keV)	I_s (eV b)	$g\Gamma_0$ (meV)	$g\Gamma_0^{red}$ (meV/MeV^3)	$B(M1)\uparrow$ (μ_N^2)
3520	0.62(12)	2.00(38)	0.05(1)	0.004 (1)
3530[b]	0.56(14)	1.82(45)	0.04(1)	0.004 (1)
3537	0.67(14)	2.17(47)	0.05(1)	0.004 (1)
3596	0.55(14)	1.84(49)	0.04(1)	0.003 (1)
3673[a]	0.80(17)	2.79(60)	0.06(1)	0.005 (1)
3678	1.96(25)	6.90(90)	0.14(2)	0.012 (2)
3682	1.29(24)	4.56(85)	0.09(2)	0.008 (2)
3685	0.71(23)	2.50(81)	0.05(2)	0.004 (1)
3732[a]	0.75(14)	2.71(51)	0.05(1)	0.005 (1)
3748	0.77(17)	2.81(61)	0.05(1)	0.005 (1)
3753	1.93(26)	7.08(97)	0.13(2)	0.012 (2)
3846	0.90(18)	3.45(71)	0.06(1)	0.005 (1)
3861	0.87(29)	3.38(113)	0.06(2)	0.005 (2)
3866	1.08(26)	4.22(100)	0.07(2)	0.006 (2)
3895	0.90(19)	3.56(73)	0.06(1)	0.005 (1)
3929	1.53(26)	6.15(104)	0.10(2)	0.009 (2)
3936	0.86(22)	3.45(87)	0.06(1)	0.005 (1)
3943[a]	1.04(23)	4.21(94)	0.07(2)	0.006 (1)
3950	1.06(29)	4.30(117)	0.07(2)	0.006 (2)

[a]Alternatively an inelastic transition can be assigned, see Table VIII.

[b]Can alternatively be assigned to another state as inelastic transition, see Table VIII.

rect calibration of the incoming photon flux, these transitions have to be disentangled. For this purpose, an additional measurement was performed using a metallic ^{165}Ho target without Al disks (see Table II). By comparing the ratios of the peak areas of the ten strongest ^{165}Ho lines observed in both measurements, a relative contribution of 4–5 % of the ^{165}Ho transition to the 2982 keV ^{27}Al line could be estimated. This correction was taken into account in the analysis.

In total, 139 levels could be observed in the investigated energy range from 2 to 4 MeV, which can be ascribed to excitations in ^{165}Ho. The properties of all states for which only transitions to the $J_0^\pi = 7/2^-$ ground state could be observed are summarized in numerical form in Table IX. For 24 states, decay branchings to the first excited state ($J_f^\pi = 9/2^-$; $E_f = 95.7$ keV) and/or to the second excited state ($J_f^\pi = 11/2^-$; $E_f = 209.8$ keV) within the ground-state rotational band could be observed. The properties of these states are summarized in numerical form in Table X. For ambiguous assignments, the criteria described in the preceding section were applied.

The total detected excitation strength in the energy range from 2 to 4 MeV is comparable to that observed in ^{163}Dy. It amounts to $\Sigma_{2-4\ \mathrm{MeV}}\ g\Gamma_0^{red} = (35.7 \pm 4.2)$ meV/MeV^3 corresponding to $\Sigma_{2-4\ \mathrm{MeV}}\ B(M1)\uparrow = (3.08 \pm 0.36)\mu_N^2$, assuming exclusively $M1$ excitations.

IV. DISCUSSION

A. Comparison with previous NRF experiments

1. The ^{163}Dy (γ,γ') reaction

The scissors mode in odd-mass nuclei was first observed in previous experiments on ^{163}Dy performed at Stuttgart about 10 yr ago [10]. A concentration of dipole strength could be detected around 3 MeV of excitation energy, which fitted well into the systematics of the scissors mode in the even-even Dy isotopes [10,18]. However, the detected total strength amounted only to roughly 40% of those seen for the even-even neighbors. Similar results were obtained for ^{161}Dy [18]. On the other hand, in the odd-mass ^{155,157}Gd isotopes, a complete fragmentation of the dipole strengths was observed without any concentration [18,19]. Therefore, one aim of the present study was to look for the missing strength and the fragmentation into numerous weak excitations, which could not be detected with the sensitivity available in the NRF experiments at that time.

In Fig. 6 the dipole strength distribution in ^{163}Dy as deduced from the present experiments (lower part) is compared with that from our previous study [10] (upper part). The results from both measurements are in a fair agreement. The strength concentrations near 2.5 and 3.0 MeV were detected in both experiments, as well as the three strong, low-lying excitations at 1942, 2180, and 2213 keV, respectively. The reduced transition probabilities agree within the error bars (except for only a few cases of very weak transitions). As can be seen in the figure, due to the about one order of magnitude increased sensitivity reached in the present experiment, a huge number of weaker excitations could be detected. Whereas in 1992 only 18 excited states were found (seven of them exhibiting a decay branching), from the present study in total 161 states (39 of them with decay branchings) could be assigned. The detection of decay branchings not seen in the former experiments has led to some new assignments, and hence to some changed ground-state transition widths in

TABLE VII. Numerical results of the ^{163}Dy experiment for levels exhibiting a decay branching. Besides the quantities given in the preceding tables, the branching ratios R_{expt}, the spins J of the photoexcited levels, and the spins J_f of the fed lower-lying states ($7/2^-$: first excited state at 73.4 keV, $9/2^-$: second excited state at 167.3 keV) are given.

E_x (keV)	I_s (eV b)	$g\Gamma_0$ [meV]	R_{expt}	J_f^π	J	$g\Gamma_0^{red}$ (meV/MeV^3)	$B(M1)\uparrow$ (μ_N^2)
1465	14.54(162)	10.29(94)	0.31(5)	$7/2^-$	5/2,7/2	3.27(30)	0.283(26)
1531	2.69(33)	3.56(33)	1.66(30)	$9/2^-$	7/2	0.99(9)	0.086 (8)
1634	4.68(46)	4.34(38)	0.38(8)	$7/2^-$	5/2,7/2	0.99(9)	0.086 (7)
1942	9.91(92)	13.54(99)	0.44(6)	$7/2^-$	5/2	1.85(14)	0.160(12)
2103	0.96(23)	2.50(39)	1.61(50)	$9/2^-$	7/2	0.27(4)	0.023 (4)
2180	15.22(141)	26.99(190)	0.41(6)	$7/2^-$	7/2	2.61(18)	0.225(16)
			0.08(2)	$9/2^-$			
2191	0.94(18)	3.80(40)	2.49(57)	$7/2^-$	5/2,7/2	0.36(4)	0.031 (3)
2213[a]	13.00(178)	22.80(234)	0.42(7)	$7/2^-$	5/2,7/2	2.10(22)	0.182(19)
2242	1.61(21)	4.42(43)	1.39(27)	$9/2^-$	7/2	0.39(4)	0.034 (3)
2493	1.28(18)	7.97(65)	3.13(53)	$7/2^-$	5/2	0.51(4)	0.044 (4)
2583	0.85(20)	6.00(59)	3.36(86)	$7/2^-$	5/2,7/2	0.35(3)	0.030 (3)
2587[b]	14.59(128)	32.38(232)	0.30(4)	$7/2^-$	7/2	1.87(13)	0.162(12)
2707	2.76(28)	7.43(63)	0.45(8)	$7/2^-$	5/2,7/2	0.38(3)	0.032 (3)
2794	0.73(16)	12.27(100)	7.92(189)	$7/2^-$	7/2	0.56(5)	0.049 (4)
2812	1.94(22)	15.28(124)	1.90(36)	$7/2^-$	7/2	0.69(6)	0.059 (5)
			1.28(2)	$9/2^-$			
2819	1.63(19)	8.31(62)	1.59(24)	$7/2^-$	7/2	0.37(3)	0.032 (2)
2844[a]	0.86(20)	4.27(58)	1.62(46)	$9/2^-$	7/2	0.19(3)	0.016 (2)
2954	2.97(34)	16.20(116)	1.67(24)	$9/2^-$	7/2	0.63(5)	0.054 (4)
2958	22.04(161)	63.58(381)	0.29(3)	$7/2^-$	7/2	2.46(15)	0.212(13)
3020[b]	2.61(23)	7.84(68)	0.28(7)	$7/2^-$	5/2,7/2	0.29(3)	0.025 (2)
3075	0.76(12)	5.41(66)	2.03(46)	$7/2^-$	5/2,7/2	0.19(2)	0.016 (2)
3182	0.66(19)	35.84(255)	22.92(668)	$9/2^-$	7/2	1.11(8)	0.096 (7)
3286[b]	0.56(20)	4.15(67)	1.75(67)	$7/2^-$	5/2,7/2	0.12(2)	0.010 (2)
3351	1.09(15)	4.72(53)	0.52(13)	$7/2^-$	5/2,7/2	0.13(1)	0.011 (1)
3362	2.55(25)	11.50(94)	0.57(10)	$7/2^-$	5/2	0.30(3)	0.026 (2)
3484	0.55(12)	5.36(69)	1.15(35)	$7/2^-$	7/2	0.13(2)	0.011 (1)
			1.18(38)	$9/2^-$			
3565[a,c]	0.55(13)	4.20(62)	1.50(45)	$9/2^-$	7/2	0.09(1)	0.008 (1)
3579[c]	0.72(23)	4.90(140)	1.12(63)	$7/2^-$	7/2	0.11(3)	0.009 (3)
3614	0.56(22)	4.57(96)	1.48(67)	$7/2^-$	5/2,7/2	0.10(2)	0.008 (2)
3638[d,b]	0.47(12)	4.08(66)	1.77(59)	$9/2^-$	7/2	0.09(1)	0.007 (1)
3649	0.62(13)	8.70(109)	3.24(82)	$7/2^-$	5/2,7/2	0.18(2)	0.016 (2)
3690[b]	2.96(31)	14.20(141)	0.37(10)	$7/2^-$	5/2,7/2	0.28(3)	0.024 (2)
3771[b]	1.16(20)	11.58(127)	1.94(43)	$9/2^-$	7/2	0.22(2)	0.019 (2)
3776[a]	0.84(18)	7.39(109)	1.58(46)	$9/2^-$	7/2	0.14(2)	0.012 (2)
3791	0.83(18)	9.88(111)	2.49(63)	$9/2^-$	7/2	0.18(2)	0.016 (2)
3881	0.73(24)	8.17(140)	1.97(75)	$7/2^-$	5/2,7/2	0.14(2)	0.012 (2)
3924	0.86(22)	9.18(168)	1.90(68)	$9/2^-$	7/2	0.15(3)	0.013 (2)
3962	1.07(28)	14.34(210)	2.58(81)	$9/2^-$	7/2	0.23(3)	0.020 (3)
3991	1.42(39)	14.62(241)	1.68(57)	$9/2^-$	7/2	0.23(4)	0.020 (3)

[a]Can alternatively be assigned to another state as inelastic transition, see Table VIII.
[b]Assigned inelastic transition also can be interpreted as corresponding to a state with decay branching, see Table VIII.
[c]Assigned inelastic transition also can be assigned to another state, see Table VIII.
[d]Alternatively a further inelastic transition can be assigned, see Table VIII.

TABLE VIII. Numerical results of the ^{163}Dy experiment. Alternative interpretations of peaks as elastic and inelastic transitions for levels exhibiting a decay branching. The quantities given are the same as in Table VII, see text.

E_x (keV)	I_s (eV b)	$g\Gamma_0$ (meV)	R_{expt}	J_f^π	J	$g\Gamma_0^{red}$ (meV/MeV^3)	$B(M1)\uparrow$ (μ_N^2)
2140	4.59(45)	5.47(54)				0.56(6)	0.048 (5)
2287	1.44(20)	20.83(259)	10.58(207)	$7/2^-$	7/2	1.74(22)	0.151 (19)
2514	3.76(37)	7.72(67)	0.27(6)	$7/2^-$	7/2	0.49(4)	0.042 (4)
2587	14.59(128)	25.41(222)				1.47(13)	0.127 (11)
2677	1.00(16)	1.87(31)				0.10(2)	0.008 (1)
2918	4.15(33)	11.25(88)	0.24(6)	$7/2^-$	7/2	0.45(4)	0.039 (3)
2946	0.65(16)	6.60(59)	3.80(99)	$7/2^-$	5/2,7/2	0.26(2)	0.022 (2)
3020	2.61(23)	6.20(55)				0.23(2)	0.020 (2)
3212	0.85(12)	40.44(280)	19.67(312)	$9/2^-$	7/2	1.22(9)	0.105 (7)
3286	0.56(20)	1.57(56)				0.04(2)	0.004 (1)
3471	0.55(11)	3.69(52)	1.21(34)	$7/2^-$	7/2	0.09(1)	0.008 (1)
3579	0.72(23)	2.39(76)				0.05(2)	0.005 (1)
3604	1.38(20)	6.82(85)	0.49(14)	$7/2^-$	5/2,7/2	0.15(2)	0.013 (2)
3610	0.82(16)	2.77(56)				0.06(1)	0.005 (1)
3617	0.91(22)	8.46(100)	1.99(55)	$9/2^-$	7/2	0.18(2)	0.015 (2)
3638	0.47(12)	3.76(65)	1.42(50)	$7/2^-$	7/2	0.08(1)	0.007 (1)
3638	0.47(12)	1.61(43)				0.03(1)	0.003 (1)
3638	0.47(12)	6.00(82)	1.42(50)	$7/2^-$	7/2	0.13(2)	0.011 (2)
			1.60(56)	$9/2^-$			
3673	0.80(17)	5.92(157)	1.29(66)	$9/2^-$	7/2	0.12(3)	0.010 (3)
3690	2.96(31)	10.50(108)				0.21(2)	0.018 (2)
3732	0.75(14)	5.46(81)	1.16(34)	$9/2^-$	7/2	0.11(2)	0.009 (1)
3771	1.16(20)	4.29(73)				0.08(1)	0.007 (1)
3943	1.04(23)	10.55(167)	1.72(54)	$9/2^-$	7/2	0.17(3)	0.015 (2)

the energy range between 3.0 and 3.2 MeV. The lower detection sensitivity in the former measurement is also the reason that in this experiment no excitations below 1.9 MeV and above 3.2 MeV were found.

The reduced excitation widths summed up in the energy range from 2 to 4 MeV observed in the present experiment could be raised roughly by a factor of 2, from $\Sigma g\Gamma_0^{red} = 19(4)$ meV/MeV^3 [10] to $\Sigma g\Gamma_0^{red} = 38.2(42)$ meV/MeV^3.

2. The ^{165}Ho (γ,γ') reaction

A first experimental study to search for low-lying $M1$ strength in ^{165}Ho was undertaken already in 1992 at the superconducting electron linear accelerator S-DALINAC at Darmstadt where both NRF measurements and inelastic electron scattering experiments, were performed [24]. Only a few transitions below 2.4 MeV were observed, which could be explained as intrinsic single-particle excitations. However,

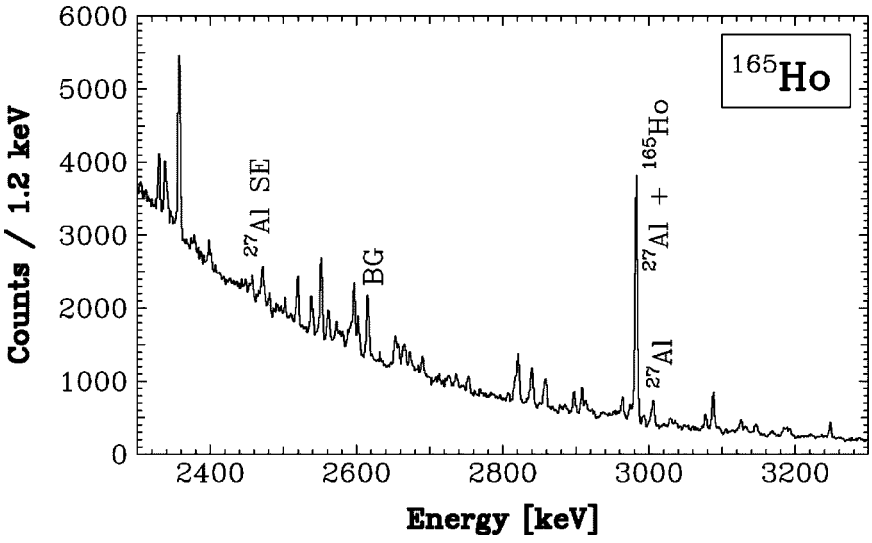

FIG. 5. Spectrum of photons scattered off ^{165}Ho in the energy range 2.3–3.3 MeV. Most of the peaks shown belong to excitations in ^{165}Ho (see text). The lines from the photon flux standard ^{27}Al and from background (BG, ^{208}Pb) are labeled.

TABLE IX. Numerical results of the ^{165}Ho experiment for levels for which only ground-state transitions could be detected. The quoted quantities are the same as in Table III.

E_x (keV)	I_s (eV b)	$g\Gamma_0$ (meV)	$g\Gamma_0^{red}$ (meV/MeV^3)	$B(M1)\uparrow$ (μ_N^2)
1381	6.67(65)	3.31(32)	1.26(12)	0.109 (11)
1389	4.48(54)	2.25(27)	0.84(10)	0.073 (9)
1409	3.30(50)	1.71(26)	0.61(9)	0.053 (8)
1416	16.66(124)	8.70(65)	3.06(23)	0.265(20)
1606	3.37(47)	2.26(31)	0.55(8)	0.047 (7)
1615	2.71(49)	1.84(33)	0.44(8)	0.038 (7)
1627	2.52(42)	1.73(29)	0.40(7)	0.035 (6)
1711	5.97(59)	4.55(45)	0.91(9)	0.079 (8)
1756	1.56(37)	1.25(29)	0.23(5)	0.020 (5)
1766	2.93(70)	2.38(57)	0.43(10)	0.037 (9)
1789	1.69(36)	1.41(30)	0.25(5)	0.021 (5)
1807	26.25(221)	22.31(188)	3.78(32)	0.327(28)
1816	10.43(87)	8.95(75)	1.49(13)	0.129(11)
1984	2.06(45)	2.11(46)	0.27(6)	0.023 (5)
2012	5.70(56)	6.01(59)	0.74(7)	0.064 (6)
2099	4.02(44)	4.61(51)	0.50(6)	0.043 (5)
2146	1.25(30)	1.50(35)	0.15(4)	0.013 (3)
2171	1.30(38)	1.59(47)	0.16(5)	0.014 (4)
2178	2.86(37)	3.53(45)	0.34(4)	0.030 (4)
2194	3.22(38)	4.04(47)	0.38(5)	0.033 (4)
2233	4.73(48)	6.13(62)	0.55(6)	0.048 (5)
2265	1.24(28)	1.66(38)	0.14(3)	0.012 (3)
2329	6.07(57)	8.57(81)	0.68(6)	0.059 (6)
2337	6.15(62)	8.75(88)	0.69(7)	0.059 (6)
2340	2.52(42)	3.59(59)	0.28(5)	0.024 (4)
2377	1.78(28)	2.62(42)	0.20(3)	0.017 (3)
2447	1.28(27)	2.00(42)	0.14(3)	0.012 (3)
2480	1.46(26)	2.33(42)	0.15(3)	0.013 (2)
2509	1.05(24)	1.73(39)	0.11(3)	0.009 (2)
2519	7.14(64)	11.79(105)	0.74(7)	0.064 (6)
2538	5.50(52)	9.22(87)	0.56(5)	0.049 (5)
2561	4.97(48)	8.49(81)	0.51(5)	0.044 (4)
2571	2.88(34)	4.95(59)	0.29(4)	0.025 (3)
2580	1.80(31)	3.11(53)	0.18(3)	0.016 (3)
2592	3.36(38)	5.87(67)	0.34(4)	0.029 (3)
2601	4.97(48)	8.75(84)	0.50(5)	0.043 (4)
2632	1.18(25)	2.14(45)	0.12(3)	0.010 (2)
2652	5.24(49)	9.60(90)	0.52(5)	0.045 (4)
2656	3.77(40)	6.93(73)	0.37(4)	0.032 (3)
2663	3.32(39)	6.13(71)	0.32(4)	0.028 (3)
2666	3.32(39)	6.14(72)	0.32(4)	0.028 (3)
2672	3.25(38)	6.03(70)	0.32(4)	0.027 (3)
2675	1.51(28)	2.81(52)	0.15(3)	0.013 (2)
2689	3.17(34)	5.97(64)	0.31(3)	0.027 (3)
2752	2.77(40)	5.46(80)	0.26(4)	0.023 (3)
2768	0.91(21)	1.82(42)	0.09(2)	0.007 (2)
2806	1.21(22)	2.48(46)	0.11(2)	0.010 (2)
2816	5.29(48)	10.91(100)	0.49(5)	0.042 (4)
2836	2.50(34)	5.23(72)	0.23(3)	0.020 (3)
2839	7.80(72)	16.36(152)	0.72(7)	0.062 (6)
2855	2.36(32)	5.00(67)	0.22(3)	0.019 (3)

TABLE IX. (*Continued*).

E_x (keV)	I_s (eV b)	$g\Gamma_0$ (meV)	$g\Gamma_0^{red}$ (meV/MeV^3)	$B(M1)\uparrow$ (μ_N^2)
2858	5.12(50)	10.89(107)	0.47(5)	0.040 (4)
2896[a]	4.60(43)	10.04(93)	0.41(4)	0.036 (3)
2913	2.81(31)	6.21(69)	0.25(3)	0.022 (2)
2917	0.99(22)	2.19(49)	0.09(2)	0.008 (2)
2921	1.04(23)	2.31(51)	0.09(2)	0.008 (2)
2951	1.23(21)	2.79(48)	0.11(2)	0.009 (2)
2958	1.41(23)	3.20(51)	0.12(2)	0.011 (2)
2963	5.17(46)	11.82(105)	0.45(4)	0.039 (4)
3035	1.15(22)	2.76(53)	0.10(2)	0.009 (2)
3077	4.74(43)	11.67(106)	0.40(4)	0.035 (3)
3105	0.92(19)	2.31(46)	0.08(2)	0.007 (1)
3120	1.47(22)	3.73(56)	0.12(2)	0.011 (2)
3131	1.97(29)	5.04(75)	0.16(2)	0.014 (2)
3134	0.98(25)	2.51(64)	0.08(2)	0.007 (2)
3144	2.43(36)	6.25(94)	0.20(3)	0.017 (3)
3147	1.51(34)	3.90(89)	0.13(3)	0.011 (3)
3167	1.25(22)	3.25(57)	0.10(2)	0.009 (2)
3183[b]	2.57(29)	6.77(77)	0.21(2)	0.018 (2)
3187	2.36(29)	6.24(78)	0.19(2)	0.017 (2)
3213	0.71(18)	1.90(48)	0.06(2)	0.005 (1)
3220	1.00(23)	2.69(63)	0.08(2)	0.007 (2)
3247	5.62(51)	15.43(139)	0.45(4)	0.039 (4)
3259	0.73(22)	2.01(61)	0.06(2)	0.005 (2)
3287	0.55(21)	1.56(59)	0.04(2)	0.004 (1)
3313	0.72(18)	2.07(52)	0.06(1)	0.005 (1)
3329	1.42(35)	4.09(100)	0.11(3)	0.010 (2)
3352	0.83(20)	2.41(58)	0.06(2)	0.006 (1)
3371	0.65(19)	1.92(55)	0.05(1)	0.004 (1)
3400	0.69(19)	2.09(56)	0.05(1)	0.005 (1)
3407	1.56(23)	4.71(71)	0.12(2)	0.010 (2)
3418	2.15(46)	6.53(139)	0.16(4)	0.014 (3)
3423	1.93(29)	5.89(87)	0.15(2)	0.013 (2)
3427	1.47(27)	4.49(82)	0.11(2)	0.010 (2)
3439	0.72(21)	2.22(66)	0.06(2)	0.005 (1)
3455	0.91(21)	2.84(64)	0.07(2)	0.006 (1)
3468	1.15(23)	3.60(72)	0.09(2)	0.007 (2)
3478	0.97(21)	3.05(67)	0.07(2)	0.006 (1)
3503	1.30(23)	4.16(73)	0.10(2)	0.008 (2)
3513	2.50(31)	8.02(99)	0.19(2)	0.016 (2)
3525	0.76(19)	2.47(61)	0.06(1)	0.005 (1)
3544	0.80(21)	2.62(68)	0.06(2)	0.005 (1)
3549	0.80(20)	2.62(67)	0.06(2)	0.005 (1)
3559	1.28(25)	4.24(82)	0.09(2)	0.008 (2)
3589	1.59(25)	5.34(85)	0.12(2)	0.010 (2)
3598	1.10(22)	3.69(76)	0.08(2)	0.007 (1)
3604	1.19(38)	4.04(129)	0.09(3)	0.008 (2)
3651	0.61(21)	2.12(72)	0.04(2)	0.004 (1)
3679	1.67(28)	5.87(98)	0.12(2)	0.010 (2)
3728	1.40(36)	5.07(131)	0.10(3)	0.009 (2)
3756	1.10(25)	4.04(91)	0.08(2)	0.007 (2)
3762	1.01(32)	3.71(116)	0.07(2)	0.006 (2)
3773	2.03(32)	7.51(120)	0.14(2)	0.012 (2)

TABLE IX. (*Continued*).

E_x (keV)	I_s (eV b)	$g\Gamma_0$ (meV)	$g\Gamma_0^{red}$ (meV/MeV^3)	$B(M1)\uparrow$ (μ_N^2)
3779	1.29(27)	4.79(99)	0.09(2)	0.008 (2)
3818	1.13(28)	4.29(107)	0.08(2)	0.007 (2)
3839	1.02(30)	3.93(113)	0.07(2)	0.006 (2)
3843	1.05(30)	4.05(115)	0.07(2)	0.006 (2)
3858	1.17(29)	4.55(111)	0.08(2)	0.007 (2)
3891	1.34(37)	5.30(147)	0.09(3)	0.008 (2)
3895	1.06(35)	4.18(139)	0.07(2)	0.006 (2)
3900	1.58(35)	6.27(137)	0.11(2)	0.009 (2)
3918	1.74(39)	6.97(156)	0.12(3)	0.010 (2)
3974	1.49(43)	6.12(175)	0.10(3)	0.008 (2)
3999	1.92(48)	8.00(200)	0.13(3)	0.011 (3)

[a]Can alternatively be assigned to another state as inelastic transition, see Table XI.
[b]Alternatively an inelastic transition can be assigned, see Table XI.

within the sensitivity limit of $0.1\mu_N^2$, no scissors mode excitation could be observed in the expected excitation energy range around 3 MeV.

A subsequent improved NRF experiment on ^{165}Ho was performed by a Darmstadt-Cologne-Rossendorf Collaboration also at the Darmstadt photon scattering facility [14] utilizing a Euroball cluster consisting of seven Ge (γ-ray) detectors, each of an efficiency of 60% relative to a 7.6 $\times$7.6 cm^2 NaI (Tl) scintillation counter, surrounded by BGO anti-Compton shields [25]. In these experiments 35 ground-

TABLE X. Numerical results of the ^{165}Ho experiment for levels exhibiting a decay branching. Besides the quantities given in the preceding tables, the branching ratios R_{expt}, the spins J of the photoexcited levels, and the spins J_f of the fed lower-lying states ($9/2^-$: first excited state at 94.7 keV, $11/2^-$: second excited state at 209.8 keV) are given.

E_x (keV)	I_s (eV b)	$g\Gamma_0$ (meV)	R_{expt}	J_f^π	J	$g\Gamma_0^{red}$ (meV/MeV^3)	$B(M1)\uparrow$ (μ_N^2)
1466	12.66(100)	8.95(65)	0.32(6)	$9/2^-$	7/2,9/2	2.84(21)	0.245 (18)
1706	11.29(93)	10.21(81)	0.23(6)	$9/2^-$	7/2,9/2	2.06(16)	0.178 (14)
1828	9.55(81)	10.26(80)	0.28(6)	$9/2^-$	7/2,9/2	1.68(13)	0.145 (11)
1903	1.97(36)	31.86(253)	18.83(381)	$9/2^-$	9/2	4.62(37)	0.399 (32)
2125	18.88(152)	26.24(186)	0.21(3)	$9/2^-$	9/2	2.74(19)	0.236 (17)
2356	22.56(182)	38.16(271)	0.19(3)	$9/2^-$	9/2	2.92(21)	0.252 (18)
2492	0.90(25)	4.79(70)	2.58(84)	$9/2^-$	7/2,9/2	0.31(5)	0.027 (4)
2551	11.84(99)	24.25(181)	0.23(4)	$9/2^-$	7/2,9/2	1.46(11)	0.126 (9)
2596	10.39(88)	21.65(164)	0.21(4)	$9/2^-$	7/2,9/2	1.24(9)	0.107 (8)
2683	1.48(24)	7.14(82)	1.76(40)	$9/2^-$	9/2	0.37(4)	0.032 (4)
2820	9.13(77)	22.49(171)	0.21(4)	$9/2^-$	7/2,9/2	1.00(8)	0.087 (7)
2973[a]	3.11(33)	9.43(93)	0.35(9)	$9/2^-$	7/2,9/2	0.36(4)	0.031 (3)
3002	1.68(32)	17.67(143)	3.84(80)	$9/2^-$	7/2,9/2	0.65(5)	0.056 (5)
3086[b]	10.02(101)	31.58(261)	0.30(4)	$9/2^-$	7/2,9/2	1.08(9)	0.093 (8)
3094	1.34(23)	8.17(94)	1.79(42)	$11/2^-$	9/2	0.28(3)	0.024 (3)
3125	3.96(38)	14.68(144)	0.50(13)	$9/2^-$	7/2	0.48(5)	0.042 (4)
3191	2.21(27)	13.89(156)	1.68(36)	$11/2^-$	9/2	0.43(5)	0.037 (4)
3237	0.78(20)	7.42(104)	3.02(92)	$11/2^-$	9/2	0.22(3)	0.019 (3)
3358	0.64(18)	4.40(87)	1.48(58)	$9/2^-$	9/2	0.12(2)	0.010 (2)
3472	2.63(32)	11.40(121)	0.41(10)	$9/2^-$	7/2,9/2	0.27(3)	0.024 (3)
3509	1.00(22)	11.51(176)	2.83(83)	$9/2^-$	7/2,9/2	0.27(4)	0.023 (4)
3702	1.43(27)	12.66(197)	1.59(47)	$9/2^-$	9/2	0.25(4)	0.022 (3)
3735	2.68(35)	13.45(159)	0.42(12)	$9/2^-$	7/2,9/2	0.26(3)	0.022 (3)
3809	0.75(31)	7.85(170)	1.92(92)	$9/2^-$	7/2,9/2	0.14(3)	0.012 (3)

[a]Can alternatively be assigned to another state as inelastic transition, see Table XI.
[b]The assigned inelastic transition can also be interpreted as corresponding to a state with decay branching, see Table XI.

TABLE XI. Numerical results of the ^{165}Ho experiment. Alternative interpretations of peaks as elastic and inelastic transitions for levels exhibiting a decay branching. The quantities given are the same as in Table X, see text.

E_x (keV)	I_s (eV b)	$g\Gamma_0$ (meV)	R_{expt} (meV/MeV^3)	J_f^π	J	$g\Gamma_0^{red}$	$B(M1)\uparrow$ (μ_N^2)
2878	0.91(22)	1.95(47)				0.08(2)	0.007(2)
2991	2.49(28)	17.47(125)	2.21(32)	$9/2^-$	9/2	0.65(5)	0.056(4)
3086	10.03(100)	24.85(249)				0.85(9)	0.073(7)
3183	2.57(29)	16.79(130)	1.81(28)	$11/2^-$	9/2	0.52(4)	0.045(4)

state transitions could be detected in the energy range between 2.5 and 4.0 MeV. Assuming an $M1$ character for all excitations, this would correspond to a total $B(M1)\uparrow$ strength of $1.54(23)\mu_N^2$. Using a fluctuation analysis technique, it was suggested that the reduction of the resolved dipole strength with respect to the even-even neighbors is hidden in the nonresonant background of the spectra [14].

In the present ^{165}Ho (γ,γ') study, the sensitivity could be increased once more by a factor of 2–3. This was possible by using three Ge (γ-ray) detectors of 100% relative efficiency in the nearest possible geometry, the highest electron currents of $\approx 250\mu$A, only limited by the thermal capacity of the bremsstrahlung radiator target, and by extending the measuring time to 110 h.

The results of the Darmstadt work [14] and of the present ^{165}Ho study are in a reasonable agreement insofar as for isolated stronger excitations the excitation energies and the integrated cross sections are in accordance within the error bars. However, the increased sensitivity of the present measurements enabled the detection of numerous additional weak peaks. Therefore, for many states new decay branchings could be observed. This led to new assignments of ground-state and inelastic transitions, and hence changed the deduced ground-state transition width (Γ_0) distribution. Furthermore, the better energy resolution in the present work allowed to resolve some peak doublets. Therefore, no one-to-one correspondence of the data from both NRF experiments can be found in general, documenting clearly the limitations of the present-day NRF technique in the case of a very high level density.

In total, 138 states below 4 MeV could be identified in the present experiments compared to 52 in the Darmstadt measurements. The total sum of the observed reduced transition widths $\Sigma_{2-4\ \mathrm{MeV}}\, g\Gamma_0^{red}$ could be increased from 27.2(38) meV/MeV^3 [14] to 35.7(42) meV/MeV^3, corresponding to total $B(M1)\uparrow$ values of $2.35(33)\mu_N^2$ and $3.08(36)\mu_N^2$, respectively, assuming an $M1$ character for all excitations.

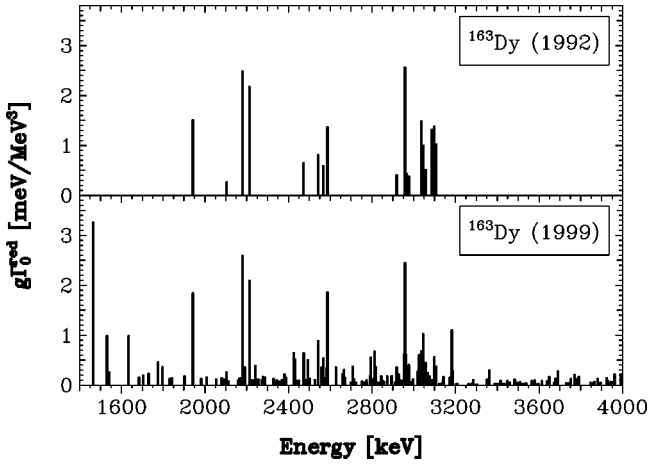

FIG. 6. Comparison of the dipole strength distribution in ^{163}Dy as deduced from the present experiments (lower part) with that from our previous study in 1992 [10] (upper part); for the discussion, see text.

B. Comparison with QPNM and sdg-IBFM calculations

The experimentally observed dipole strength distribution in ^{163}Dy can explicitly be compared with theoretical expectations. Two types of calculations were available. Soloviev and co-workers [26] studied electric and magnetic dipole excitations in several deformed odd-mass nuclei using a separable Hamiltonian within the microscopic quasiparticle-phonon-nuclear model (QPNM). In the framework of the

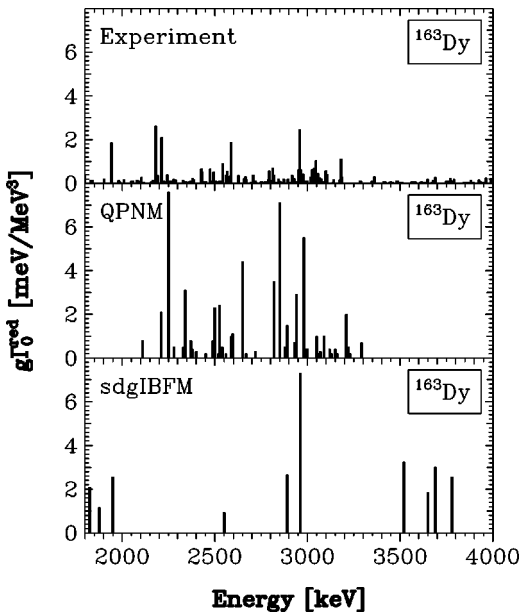

FIG. 7. Comparison of the experimentally observed dipole strength distribution in ^{163}Dy with QPNM [26] and sdg-IBFM [27] calculations.

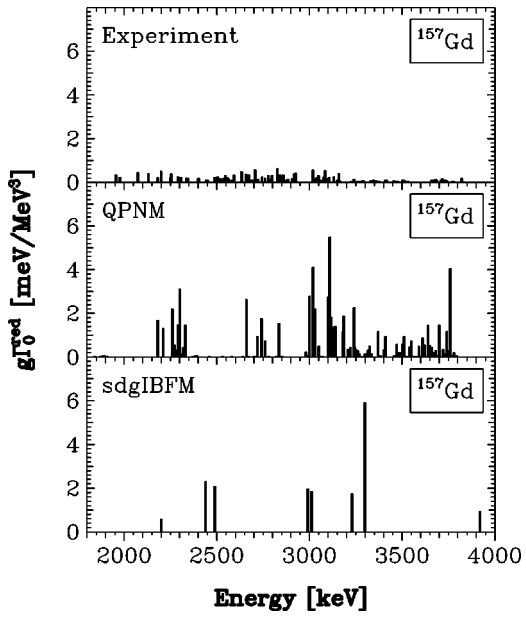

FIG. 8. Comparison of the experimentally observed dipole strength distribution in ^{157}Gd with QPNM [26] and sdg-IBFM [27] calculations.

algebraic interacting boson model extended for the description of odd-mass nuclei, the so-called sdg-interacting boson fermion model (sdg-IBFM), Devi and Kota calculated the magnetic dipole distributions in ^{157}Gd and ^{163}Dy [27].

In the Figs. 7 and 8 both calculations are compared with the present results for ^{163}Dy and former ^{157}Gd data [18], respectively. Since in the NRF experiments on odd-mass nuclei electric and magnetic dipole excitations could not be disentangled, the results of the QPNM calculations are plotted consequently for both multipolarities. In the case of the sdg-IBFM calculations, only $M1$ dipole strengths are calculated and depicted. The experimentally observed strong fragmentation of the dipole strengths in both nuclei can only be described approximately by the QPNM calculations [26], whereas the sdg-IBFM calculations [27] predict only a few states. For ^{163}Dy, the QPNM describes also quite well the strength concentrations, however, it fails to reproduce the extreme strength fragmentation in ^{157}Gd. Furthermore, the QPNM overestimates the total strengths by factors of about 2 and 4 for ^{163}Dy and ^{157}Gd, respectively. On the other hand, the total strengths calculated within sdg-IBFM agree reasonably with the experimentally observed values. However, $E1$ contributions are not included, which are expected to contribute in a non-negligible way.

C. Systematics of dipole strength distributions in odd-mass rare-earth nuclei

In this section the dipole strength distributions in odd-mass rare-earth nuclei measured at the Stuttgart photon scattering facility are summarized and discussed. Figure 9 gives an overview on the dipole strength distributions in ^{151,153}Eu (this work), ^{155,157}Gd [18,19], ^{159}Tb [19], ^{161}Dy [19], ^{163}Dy (this work), and ^{165}Ho (this work). Plotted are the products of the spin factors g times the reduced ground-state transition

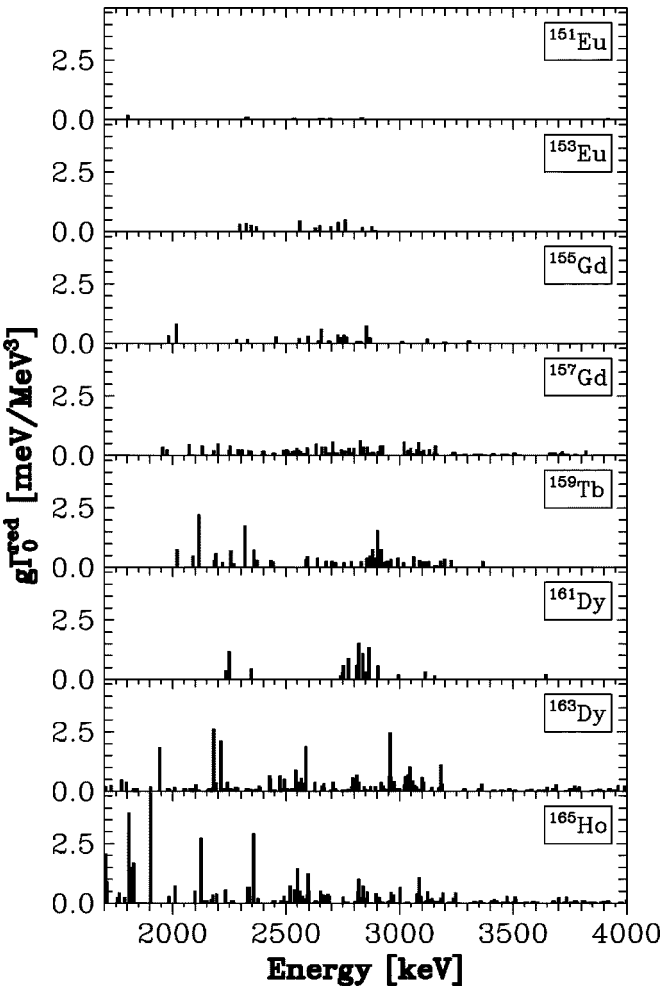

FIG. 9. Systematics of the dipole strength distributions in odd-mass rare-earth nuclei as detected in NRF experiments performed at the Stuttgart facility. The results from the present experiments on ^{151,153}Eu, ^{163}Dy, and ^{165}Ho are compared with data from previous studies [18,19]. Equal ordinate scales were chosen intentionally to demonstrate the rapidly increasing fragmentation and reduction of detectable strengths for nuclei with decreasing mass number A.

widths Γ_0^{red}, which are proportional to the reduced excitation probabilities $B(E1)\uparrow$ or $B(M1)\uparrow$, see Eqs. (3) and (4), as a function of the excitation energy. In the lighter isotopes ^{151,153}Eu and ^{155,157}Gd, only very weak transitions could be observed. These isotopes do not exhibit any strength concentrations. The number of detectable transitions obviously appears to increase with the mass number A; e.g., in ^{157}Gd about 90 weak transitions could be detected to be spread rather homogeneously over the entire excitation energy range from 2 to 4 MeV. In the next heavier investigated nucleus ^{159}Tb, about the same number of states was observed, however, there are two bumps of strength concentrations visible at about 2.3 and 2.9 MeV, respectively. These strength concentrations were also found in ^{161}Dy, however, the continuum of weak transitions is not seen. The reason for this is purely experimental, since in this early experiment [18] the sensitivity was by far the lowest of all presented measurements. This could be confirmed by the new investigation of

TABLE XII. Compilation of summed $M1$ scissors mode strengths observed in odd-mass rare-earth nuclei as detected in NRF experiments in Stuttgart. In the third column once again the observed summed reduced dipole widths are given. The fourth column shows the portions attributed to the scissors mode as deduced applying Eq. (9). In the last two columns a comparison of the detected total $B(M1)\uparrow$ scissors mode strengths and the values expected from sum rule considerations [4] is depicted, see text.

Nucleus	Reference	$\Sigma_{2\ \mathrm{MeV}}^{4\ \mathrm{MeV}}\, g\Gamma_0^{red}$ (meV/MeV^3)	$\Sigma_{Sciss}\, g\Gamma_0^{red}(M1)$ (meV/MeV^3)	$\Sigma_{Sciss}^{expt}\, B(M1)\uparrow$ (μ_N^2)	$\Sigma_{Sciss}^{theo}\, B(M1)\uparrow$ (μ_N^2)
^{151}Eu	This work	0.95	0.33	0.03	0.72
^{153}Eu	This work	3.55	2.60	0.22	2.39
^{155}Gd	[19]	6.18	3.95	0.34	2.35
^{157}Gd	[18]	18.5	11.8	1.02	2.42
^{159}Tb	[19]	21.8	13.7	1.18	2.51
^{161}Dy	[18][a]	10.2	9.14	0.79	2.42
^{163}Dy	This work[b]	38.2	23.5	2.03	2.21
^{165}Ho	This work	35.7	14.7	1.27	2.63

[a]The sensitivity of the measurement on ^{161}Dy was significantly lower than in other measurements.
[b]The sensitivity of the measurement on ^{163}Dy was significantly higher than in other measurements.

^{163}Dy. The data exhibit an extreme fragmentation of the strength in about 160 transitions, most of them below the sensitivity limit of our former measurements [10]. However, besides a flat distribution of weak transitions, two clearly pronounced strength concentrations near 2.5 and 3 MeV are visible. For ^{165}Ho, the strength bumps are less pronounced, but the fragmentation is as high as in ^{163}Dy. In addition, in ^{165}Ho some stronger excitations below 2.5 MeV could be observed, which are predicted to be single-particle excitations [24].

When trying to extract from the measured dipole strength distributions the portions of strength of interest, which should be ascribed to the $M1$ scissors mode, two problems arise. In the first place (as already pointed out), in NRF experiments on odd-mass nuclei, no parity determinations are possible. Second, in these isotopes exhibiting a rather flat dipole strength distribution, it is not straightforward to select the correct excitation energy range, over which the scissors mode is assumed to be spread. To overcome this dilemma we choose a pragmatic procedure following the lines as proposed and applied in a recent study [13] to check the fluctuation analysis of photon scattering spectra [12], which allows to estimate the percentage of undetected dipole strength hidden in the continuous background in these spectra due to the extreme fragmentation. The basic assumption is a smooth behavior of the scissors mode properties in both, odd-mass nuclei and the neighboring even-even isotopes. In the even-even neighbors, parity assignments are possible, and hence the ratio of $M1$ to $E1$ strength can be deduced. Furthermore, the $M1$ scissors mode strengths are rather concentrated in a small range of excitation energy. Therefore, the integration interval to extract the total $M1$ scissors mode strength in odd-mass nuclei can be fixed from these data (2.7–3.7 MeV). To estimate the $M1$ to $E1$ strength ratios, we use data from previous NRF experiments on the neighboring even-even nuclei ^{150,152}Sm [28], ^{156,158}Gd [29], ^{160}Dy [23], ^{162}Dy [30], and ^{164}Dy [18].

It can be shown that the percentage $\Sigma_{2-4\ \mathrm{MeV}}\, g\Gamma_0^{red}(M1)/\Sigma_{2-4\ \mathrm{MeV}}\, g\Gamma_0^{red}(\mathrm{tot})$ of $M1$ strength in the energy range 2–4 MeV amounts to 65–90 % of the total dipole strengths for the even-even nuclei with $A \geqslant 152$ [31]. With this information from the neighboring even-even nuclei ("*e-e* cores") we can estimate the detected scissors mode strengths $\Sigma_{Sciss}\, g\Gamma_0^{red}$ by multiplying the total dipole strength $\Sigma_{2-4\ \mathrm{MeV}}\, g\Gamma_0^{red}$ with the relative portion of $M1$ strengths, as observed in the neighboring even-even core nuclei, and by taking into account the excitation energy range appropriate to the scissors mode, see Eq. (9),

$$\sum_{Sciss} g\Gamma_0^{red} = \sum_{2\ \mathrm{MeV}}^{4\ \mathrm{MeV}} g\Gamma_0^{red} \left(\frac{\sum_{2\ \mathrm{MeV}}^{4\mathrm{MeV}} g\Gamma_0^{red}(M1)}{\sum_{2\ \mathrm{MeV}}^{4\ \mathrm{MeV}} g\Gamma_0^{red}(\mathrm{tot})} \right)_{e\text{-}e\ core} \times \left(\frac{\sum_{2.7\ \mathrm{MeV}}^{3.7\ \mathrm{MeV}} B(M1)\uparrow}{\sum_{2\ \mathrm{MeV}}^{4\ \mathrm{MeV}} B(M1)\uparrow} \right)_{e\text{-}e\ core} . \quad (9)$$

In Table XII the numerical data concerning the scissors mode detected in Stuttgart NRF experiments are summarized. An error estimate is difficult. The detected total strengths have errors in the order of 10%. However, the systematic uncertainties for the correction ratios with even-even core data should be more decisive. In the last two columns the total observed scissors mode strengths $\Sigma_{Sciss}^{expt}\, B(M1)\uparrow$ are compared with the corresponding values $\Sigma_{Sciss}^{theo}\, B(M1)\uparrow$ as theoretically expected from sum rule considerations. Explicitly, we use the sum-rule for the total $M1$ scissors mode strength as derived by Lo Iudice and Richter [4] for even-even nuclei,

$$B(M1)\uparrow \approx 0.0042 \left(\frac{4NZ}{A^2} \right) \omega_{Sciss} A^{5/3} (g_p - g_n)^2 \delta^2(\mu_N^2), \quad (10)$$

with ω_{Sciss} the mean energy of the scissors mode, δ the nuclear deformation parameter, A the mass number, and the nucleon g factors g_n and g_p (for a numerical estimate we used as in Ref. [4] g factors $g_n=0$ and $g_p=2Z/A$). This formula contains no free parameters and predicts correctly the absolute strengths for the scissors mode in both well-deformed and transitional even-even nuclei, and in particular the dependence of the total strengths on the square of the deformation parameter δ [32,33]. The complete exhaustion of the sum rule by the experimentally observed strengths may be interpreted such that in the NRF experiments nearly all orbital $M1$ excitations (scissors mode) in even-even nuclei have been observed.

Therefore, the sum-rule predictions for the odd-mass isotopes should be a possible criterion for the detected $M1$ strengths. It may be noted that sum-rule predictions have also been derived for odd-mass rare-earth nuclei within the IBFM [34], although not for the nuclei investigated here. Nevertheless, these results suggest $B(M1)$ strengths similar or even slightly larger than for even-mass nuclei. Even if the data summarized in Table XII were obtained in NRF experiments of quite different sensitivity, one trend is clearly evident. The experimentally observed $M1$ strengths increase with the mass number A. This is in contradiction to the sum-rule expectations and the experimental findings in the even-even nuclei. A natural explanation could be an increasing fragmentation of the scissor mode strength in the lighter isotopes, spreading the strength over many weak excitations, which cannot be detected by present-day photon scattering experiments. The important contribution of these numerous weak transitions to the total sum could be demonstrated by the present measurements on ^{163}Dy. The improvement of the detection limit by a factor of 20 led to a doubling of the detected total dipole strength as compared to our previous NRF study of ^{163}Dy [10]. Therefore, only the total dipole strength in ^{163}Dy as observed in the experiment with the highest sensitivity and ascribed to the scissors mode exhausts within the uncertainties the sum-rule predictions (see Table XII). From this one may be tempted to conclude that the problem of the so-called missing scissors mode strength in odd-mass deformed nuclei is simply due a lack of sensitivity in most of the NRF experiments so far. On the other hand, this would contradict the basic assumptions of the statistical analysis of (γ,γ) spectra of odd-mass rare-earth nuclei [12,13], which assumes that individual levels overlap and are therefore, at least partly, unresolvable. It is important to perform such an analysis for the new data presented here.

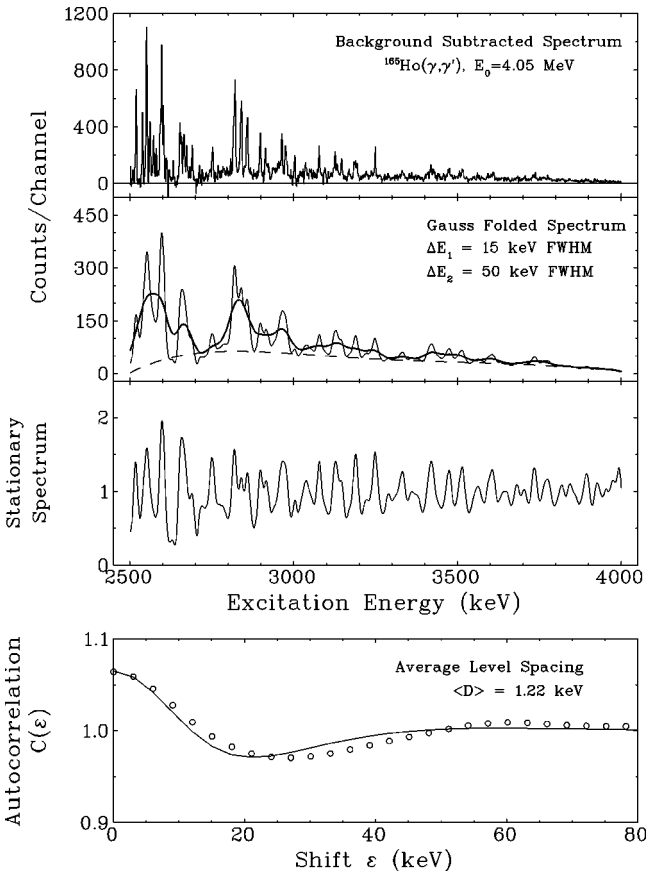

FIG. 10. Fluctuation analysis of the ^{165}Ho(γ,γ') spectrum, see text. Top row: Background subtracted spectrum. Second row: Spectrum folded with Gaussians of width $\Delta E_1=15$ keV (thin solid line), and additionally with $\Delta E_2=50$ keV (thick solid line). The dashed line indicates the optimum unresolved strength added to obtain an optimum agreement with the prediction of Eq. (12). Third row: Ratio of the thin and thick curves above, the so-called stationary spectrum showing the local fluctuations. Bottom row: Autocorrelation function of the spectrum (open circles) compared with the theoretical prediction of Eq. (12) using the parameters of model *A* in Table XIII (solid line).

V. FLUCTUATION ANALYSIS OF THE ^{163}Dy(γ,γ') AND ^{165}Ho(γ,γ') SPECTRA

In the following, a fluctuation analysis is presented for the data obtained on ^{163}Dy and ^{165}Ho. These cases are particularly interesting because they can be compared to previous results [12,14], thereby providing an important test of the method. The new results presented above demonstrate that the extracted total dipole strengths increase with improved sensitivity and energy resolution qualitatively in line with the predictions of the statistical analysis. Somewhat contradictory, the new measurement for ^{163}Dy seems to exhaust the total expected scissors mode strength in individual transitions. However, one should be aware that in the neighboring nucleus ^{164}Dy, significant mixing with spin strength has been observed, leading to an unusually high total $M1$ strength around 3 MeV [35]. Thus, possible spin contributions may also influence the observations in ^{163}Dy.

The basic ideas underlying the fluctuation analysis technique are described in Ref. [36] and its application to inelastic electron scattering spectra is presented, e.g., in Ref. [37]. Because the peculiarities of the analysis of photon scattering spectra is discussed in detail in Ref. [14], only the most important features are briefly summarized here: A so-called stationary spectrum is extracted from a sliding average of the smoothed experimental spectrum. It then only contains the fluctuations around the local mean. A measure of the fluctuations is given by the autocorrelation function of the stationary spectrum,

$$C(\varepsilon)=\langle S(E_x)S(E_x+\varepsilon)\rangle, \tag{11}$$

where the brackets indicate averaging over the interval for which the analysis is performed, and ε is the shift parameter. This experimental information on fluctuations is compared to a theoretical autocorrelation function $C(\varepsilon)$ that depends on the average level spacing $\langle D\rangle$ and the knowledge of the probability distributions for the intensities and the spacing of neighboring excitations entering into the parameter α,

$$C(\varepsilon)=1+\langle D\rangle\alpha f(\sigma_<,\sigma_>,\varepsilon). \tag{12}$$

Here, the function $f(\sigma_<,\sigma_>,\varepsilon)$ depends only on the preparation of the spectrum by folding with Gaussians of widths ($\sigma_<$ and $\sigma_>$) described below.

A number of important aspects can be probed with the new analysis. (1) Do similar start parameters lead to comparable results for different spectra? (2) How far are basic assumptions on the statistical properties of the spectra underlying the method justified? (3) Does the statistical approach also apply to a nucleus like ^{163}Dy with an unusual fragmentation pattern in which a large part of the strength is concentrated in a few transitions?

A. Stationary spectra and input parameters

1. Preparation of the spectra

The following steps are performed to obtain stationary spectra: Based on the analysis of individual transitions, one obtains approximations for the nonresonant background in various energy intervals from fitting the resolved peaks. The individual energy intervals of the fitted background are combined and smoothed by averaging out steps at the edges of the intervals. The scale upon which the averaging is done has to be of the order of the second smoothing which is used in the determination of the stationary spectrum. This smooth curve is then subtracted from the original spectrum. All discrete transitions from the calibration material and background lines are removed. Furthermore, all escape peaks and inelastic transitions have to be removed in order to avoid a multiple counting of the number of excited levels. The resulting spectrum is displayed in the top part of Fig. 10 for the example of ^{165}Ho. The contributions of finite statistics to the fluctuations can be effectively suppressed by folding with a Gaussian of width $\Delta E_1=15$ keV FWHM (full width at half maximum; thin line in the second row of Fig. 10). This also assures that the condition $\langle D\rangle<\Delta E$ is valid over the whole excitation energy region investigated. A sliding average is determined with $\Delta E_1=50$ keV FWHM (thick line in the second row of Fig. 10). The ratio of both spectra, the stationary spectrum, is shown in the third row and carries only the information about local fluctuations of the cross sections around the mean value.

2. Level densities

Different models can be used to extract the level densities needed for the application of Eq. (12). Empirical parametrizations like the ''constant temperature model (CTM)'' [38] and the ''backshifted Fermi gas model (BFGM)'' [39] exist, whose parameters have been determined either in global fits to large mass ranges or partly in fits to individual nuclei. Alternatively, a variety of microscopic calculations can be found. One recent example is the work of Demetriou and Goriely [40] using a Hartree-Fock plus BCS model. For compatibility with previous analyses, we restrict ourselves to the CTM and BFGM values obtained with the parameters from Ref. [41]. The spin dependence due to the different angular momenta allowed for dipole transitions $J_f=|J_0\pm1|$ is taken into account by the spin cutoff parameters in the CTM and BFGM, respectively. An inherent assumption of the empirical models used here are equal level densities of positive and negative parity states. This is questionable at low excitation energies where the single-particle spectrum may still play a role (see, e.g., Ref. [42]). Thus, the ratio is determined here by taking the average over the $M1$ and $E1$ strengths observed in the even-even neighbors.

TABLE XIII. Parameters of the fluctuation analysis on ^{165}Ho (for models *A* and *B*) and ^{163}Dy (model *A* only). The quantities $\langle B\rangle$ and $\langle N\rangle$ denote the mean of the ratio of summed $M1$ and $E1$ strengths, and the ratio of the number of $M1$ and $E1$ excitations in the neighboring even-mass nuclei.

Quantity	^{165}Ho		^{163}Dy
	A	*B*	*A*
Average level spacing $\langle D\rangle$ (keV)	1.22	0.41	1.21
Mean dipole strength ratio $\langle B\rangle$	1.77	1.77	3.38
Mean level number ratio $\langle N\rangle$	1.23	1.23	1.67
Variance α	2.52	2.93	3.00

In the previous analysis [14], an effective level density was used based on an analysis of the nearest neighbor spacing distributions (NNSD), suggesting that only the multipole character plays a role and the densities of states with allowed *J* values should be averaged rather than added. This leads to an effective level spacing increased by a factor of 2–3. We call this approach *A* in the following. Subsequently, more refined studies of the NNSD of scissors mode states in even-mass nuclei [15] showed that this interpretation is unfounded because the NNSD extracted for the data ensemble of dipole transitions in odd-mass heavy nuclei are strongly influenced by the finite sensitivity limit and detector resolution. Instead, the full level density including all allowed final states needs to be considered. This will be referred to in the following as analysis *B*. To quantify errors on the final result induced by the level density, a 10% uncertainty is allowed for. This corresponds to the maximum differences between the CTM and BFGM predictions. Note, however, that the level densities predicted by the calculations of Ref. [40] are generally higher for the nuclei under investigation exceeding a factor of 2 for certain *J* values.

3. Level spacing and intensity distributions

A further parameter entering the theoretical autocorrelation function is the sum of the variances of the distributions describing the nearest neighbor level spacing and the transition strengths. Based on the findings of Ref. [15], the previ-

ous interpretation of the NNSD of dipole excitations in odd-mass nuclei as a superposition of two Wigner-Dyson distributions can no longer be upheld. It is unclear whether the underlying distributions of $M1$ and $E1$ excitations (approach A) or the distributions of the states excited by dipole transitions (approach B) are of Wigner or Poisson type, or somewhere in between. However, the influence of the NNSD on the total variance is small, and is considered in the estimate of uncertainties. In calculation A, we use the superposition of two Wigner distributions in order to maintain consistency with previous analyses. For calculation B, the average of a superposition of six Wigner-type and six Poisson-type distributions (corresponding to the six possible J^π values) is used.

The intensity distributions of the reduced widths are of Porter-Thomas (PT) type if the underlying NNSD is of Wigner type. We assume a superposition of two PT distributions for analysis A as used previously. There is no prediction or experimental data for the intensity distribution corresponding to a Poisson-type NNSD. For simplicity, we assume in analysis B a superposition of six PT distributions.

B. Results for ^{165}Ho

A summary of the input parameters for the analysis of ^{165}Ho resulting for models A and B is presented in Table XIII. The excitation energy interval $E_x = 2.5$–4.0 MeV is taken into account in the calculation of the mean dipole strength ratio $\langle B \rangle$ to comply with the previous analysis. Accordingly, the mean level spacing is averaged over the same interval. The ratio of $M1$ and $E1$ transitions in the even-mass neighbors is determined in a slightly different way with respect to the analysis described in Ref. [14]. The assigned parity is in most cases based on the K quantum number of the excited state deduced from the Alaga predictions for the intensity ratio of the decay to the ground state (g.s.) and 2_1^+ state. In well-deformed nuclei, $\Delta K = 1$ transitions correspond to $J^\pi = 1^+$ excited states, and $\Delta K = 0$ transitions to $J^\pi = 1^-$ states. However, in all nuclei investigated with NRF, one finds pure g.s. transitions without a corresponding inelastic line populating the 2_1^+ state. In Ref. [14], these were interpreted as $M1$ excitations, while they are completely excluded from the determination of the $M1/E1$ ratio here, in accord with Ref. [15]. The resulting theoretical autocorrelation function for model A is displayed as a solid line in the bottom part of Fig. 10.

The unresolved experimental dipole strength hidden in the background is now extracted by an iterative procedure. The amount of hidden strength is determined by the requirement that the value $C(\epsilon = 0)$ deduced from the stationary spectrum equals the theoretical prediction. The data are analyzed in 300 keV steps; and assuming a smooth function, the energy dependence over the entire energy range can be determined with little adjustment ($< 5\%$) of the values obtained for the smaller intervals. The open circles in the bottom part of Fig. 10 show the resulting experimental autocorrelation function after adding the optimum background (dashed line in the second row of Fig. 10). After adjusting the background, the total cross section, if assumed to be dipole strength, corresponds to $\Sigma g \Gamma_0^{red} = 52.2$ meV/MeV^3 for the energy interval 2.5–4 MeV. One finds indeed that the background deduced from the fluctuation analysis is lower than the one obtained from the analysis of resolved transitions, which served as the starting point for the fluctuation analysis. Therefore, resonant unresolved strength is present in the background of the spectrum. The dashed smooth curve in the second panel of Fig. 10 shows the difference between the background subtracted spectrum and the additional background extracted within the fluctuation analysis.

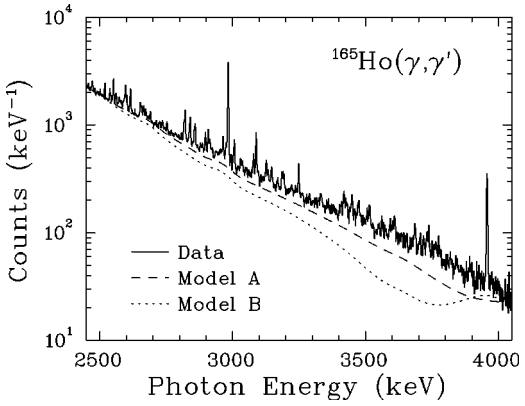

FIG. 11. Spectrum of the ^{165}Ho(γ,γ') reaction (in logarithmic scale) with the nonresonant background shapes predicted by the fluctuation analysis using the parameter sets of model A (long-dashed line) or model B (short-dashed line) from Table XIII.

The influence of the different parameters on the uncertainty of final result has been estimated by variations within reasonable limits. The individual contributions are (1) variation of the level density by 10%: change of $\Sigma g \Gamma_0^{red}$ by $(+7,-6)\%$, (2) noise (see Ref. [13]): $\pm 4\%$, (3) variation of ΔE_1 by ± 5 keV: $(-10,+8)\%$, (4) variation of ΔE_2 by ± 10 keV: $(-5,+1)\%$, (5) local deviations in fit to small (300 keV) intervals: $\pm 2\%$, (6) variation of α between 2.46 and 3.0: $(-14,0)\%$, (7) background subtraction in the spectrum (see [13]): $\pm 10\%$, (8) errors in peak removing (see Ref. [13]): $\pm 4\%$, and (9) choice of interval widths: $\pm 5\%$.

If the individual error contributions are added in quadrature, a total uncertainty of $(+17,-18)\%$ is estimated. An additional systematic uncertainty comes from the unknown statistical nature of the NNSD. If a Poisson type instead of a Wigner type is assumed, the extracted strength decreases by additional 14%.

The final result $\Sigma g \Gamma_0^{red} = (52 \pm 9)$ meV/MeV^3 is equivalent to $\Sigma B(M1) = (4.5 \pm 0.8)\mu_N^2$, assuming a pure $M1$ character of the observed dipole strength. However, as discussed above it is more appropriate to take the value $\langle B \rangle$ given in Table XIII for the unknown $M1/E1$ ratio leading to $\Sigma B(M1) = (2.9 \pm 0.5)\mu_N^2$. This result agrees within error bars with $\Sigma B(M1) = (3.5^{+0.8}_{-1.0})\mu_N^2$ deduced from the analysis of the spectrum previously measured at the S-DALINAC [14].

The analysis of model B leads to $\Sigma g \Gamma_0^{red} = (82^{+13}_{-14})$ meV/MeV^3 equivalent to $\Sigma B(M1) = (7.1^{+1.1}_{-1.2})\mu_N^2$ for pure $M1$ strength, respectively, $\Sigma B(M1) = (4.5^{+0.7}_{-0.8})\mu_N^2$ taking the

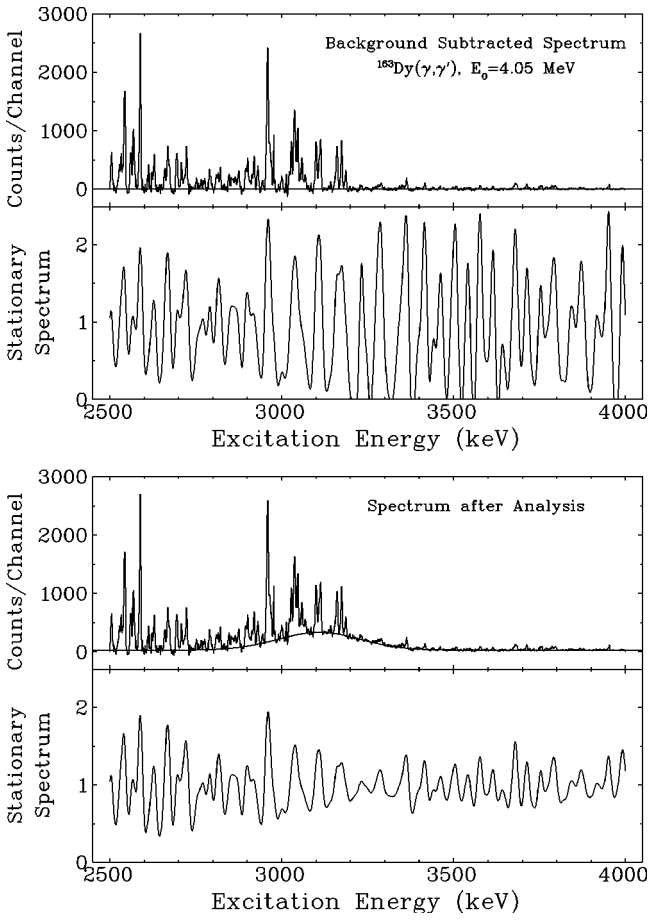

FIG. 12. Fluctuation analysis of the ^{163}Dy(γ,γ') spectrum, see text. Upper part: Background-subtracted spectrum and resulting stationary spectrum without adding additional unresolved strength. Lower part: The same after adding nonresonant strength to obtain optimum agreement with the theoretical prediction of Eq. (12) using the parameters of model *A* in Table XIII.

$\langle B\rangle$ value from Table XIII. The individual contributions to the total error of $(+16,-18)\%$ are (only differences to model *A* are shown) (1) variation of the level density by 10%: change of $\Sigma g\Gamma_0^{red}$ by $(\pm 5)\%$, (2) variation of ΔE_1 by ± 5 keV: $(-6,+3)\%$, (3) variation of ΔE_2 by ± 10 keV: $(-4,+1)\%$, (4) local deviations in fit to small (300 keV) intervals: $\pm 7\%$, and (5) variation of α between 2.73 and 3.15: $(-14,0)\%$. The much larger total strength is easily understood. Whereas α is nearly unchanged, the level density is much higher, thereby decreasing the product $\alpha\langle D\rangle$ in Eq. (12). Additional strength has to be added to reduce the fluctuations in the stationary spectrum to the required level.

A distinction between the two different models is possible by investigating the shape of the resulting experimental background. Figure 11 shows the spectrum of the ^{165}Ho(γ,γ') reaction (in logarithmic scale), with the background shapes deduced from models *A* and *B* as dashed and dotted lines, respectively. The nonresonant background in NRF experiments is known to be smooth and to decrease monotonically towards the end point energy. While the background extracted from model *A* reproduces this behavior and levels off at the end point energy, the background deduced

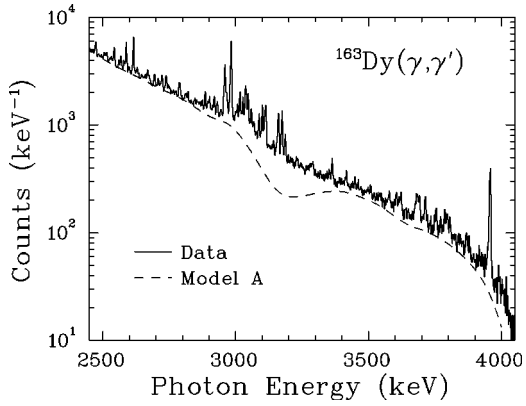

FIG. 13. Spectrum of the ^{163}Dy(γ,γ') reaction (in logarithmic scale) with the nonresonant background shape predicted by the fluctuation analysis using the parameter set of model *A* (long-dashed line) from Table XIII.

from *B* exhibits a pronounced dip a few hundred keV below the end point. Such a result can be ruled out to be unphysical. Thus, despite being based on the introduction of an ''effective'' level density, which can be no longer justified in view of the recent statistical analysis of the scissors mode states in even-mass nuclei, model *A* provides a proper description of the background shape as well as a total scissors mode strength in accordance with that in the even-mass neighbors and sum-rule predictions.

Two interpretations are possible. On one hand, the result could be explained assuming a significantly larger variance, implying an extremely broad intensity distribution. However, basic considerations suggest that the intensity distribution corresponding to a Poisson-type NNSD should have a smaller variance compared to a PT distribution, which leaves such an explanation unlikely. On the other hand, the level spacing could indeed be considerably larger (i.e, the level density lower) than suggested by the empirical models demonstrating that for a known background, the fluctuation analysis technique may be an attractive method to extract spin and parity separated level densities. It is worth noting that the recent microscopic calculations in Ref. [40] predict even higher level densities than the BFG and the CT models, for all spins and parities important for this analysis. If one assumes a purely statistical fragmentation of the scissors mode on the available phase space, we find that the predicted level densities in Ref. [40] are too high. On the other hand, it could be possible that the scissors mode does not fragment onto all states with the allowed J^π values. Such a behavior would correspond to a localization of the scissors mode in the phase space, and might be connected to a randomized NNSD and the collectivity of the mode.

C. Results for ^{163}Dy

The input parameters for ^{163}Dy are given in Table XIII. The analysis is performed for model *A* only for reasons explained below. The background-subtracted ^{163}Dy(γ,γ') spectrum and the resulting stationary spectrum (without adding additional unresolved parts) are displayed in the upper part of Fig. 12. The pronounced fluctuations of the stationary

spectrum indicate that considerable resonant strength should be hidden in the nonresonant background. The result of the fluctuation analysis is presented in the lower part of Fig. 12. A concentration of strength around 3.2 MeV, just above the prominent resolved transitions, is needed to reduce the amount of fluctuations and reproduce the decreasing amplitude in the stationary spectrum expected from the increasing level density. The distribution of additional strength indicated by the dashed line differs strongly from the one obtained for ^{165}Ho.

The deduced shape of the nonresonant spectrum part is plotted in Fig. 13. From the arguments given above for the case of ^{165}Ho it is clear that the pronounced dip around 3.2 MeV is unphysical. The problem would be even more severe using a set of parameters typical for model *B* because the larger level density reduces fluctuations in the stationary spectrum and even more resonant strength would be needed. One must conclude that the statistical assumptions that form the basis of the fluctuation analysis fail for ^{163}Dy. Already the statistical model discussed in Refs. [12,14] significantly overestimated the degree of fragmentation observed experimentally for ^{161,163}Dy, while providing a reasonable description for most other cases. Also for the even-mass Dy isotopes, one finds a minimum of the degree of fragmentation of the scissors mode [43] suggesting an origin in the underlying shell structure. Although a smooth behavior of the scissors mode properties is experimentally found and theoretically suggested by the successful interpretation in terms of sum rules, sudden changes between neighboring isotopes or isotones may occur. Examples are the abrupt onset of spin strength when going from ^{162}Dy to ^{164}Dy [23,35] and the change of the scissors mode properties in ^{194,196}Pt [44,45].

VI. CONCLUSIONS

An experimental study of the (γ,γ) reaction at excitation energies below 4 MeV was presented for the deformed, odd-mass, rare-earth nuclei ^{151,153}Eu, ^{163}Dy, and ^{165}Ho. A large amount of new spectroscopic information on dipole transitions in these nuclei could be extracted. Including previous data on ^{155,157}Gd, ^{159}Tb, and ^{161}Dy, an experimental systematics can be established. The dipole strength distributions are generally very fragmented, with the exception of ^{163}Dy. Assuming that the $M1/E1$ strength ratio can be approximated by the average over the neighboring even-mass nuclei, the total scissors mode strength can be extracted. If compared to sum-rule expectations, only a fraction of the strength is detected, increasing with deformation and mass number *A* below midshell. Again, ^{163}Dy is an exception where the total $B(M1)$ value agrees with the sum-rule prediction within the experimental and theoretical uncertainties. The comparison of the present data on ^{163}Dy, and ^{165}Ho, with previous results also makes clear that the amount of dipole strength experimentally observed is sensitive to the experimental energy resolution and the detection limits.

While a part of the experimentally missing strength may be explained to be due to the experimental conditions, the high level densities in these nuclei also imply that a certain fraction may be unresolved and therefore treated as nonresonant background in the decomposition of the spectra. The latter part can be extracted by a fluctuation analysis technique based on the knowledge of the level densities and the statistical properties of the level spacing and intensity distributions of the excited dipole modes. The new data on ^{165}Ho provide an important test case for the application of this method to photon scattering spectra. For similar input parameters, the analysis of two independent measurements of the ^{165}Ho(γ,γ') reaction with different end point energies, energy resolution, and sensitivity limits lead to consistent predictions for the total scissors mode strength within the uncertainties of the method. It is, furthermore, demonstrated that the predicted nonresonant background shape is sensitive to the level densities and/or the variance of the intensity distributions, which allows to exclude certain parameter ranges as unphysical. Unless one assumes a very unusual, extremely broad intensity distribution, the present results suggest that the density of levels excited in the (γ,γ') reaction is significantly (factor of $2-3$) smaller than predicted by global parameter sets of empirical models, or that the scissors mode fragments only onto a fraction of the states that are predicted in the investigated energy interval.

Finally, the new measurement of ^{163}Dy confirms impressively the exceptional character of the scissors mode strength distribution in this nucleus. The fluctuation analysis produces unphysical background shapes. This may either be due to a breakdown of the underlying statistical assumptions or result from a lack of unresolved strength suggested by the large $B(M1)$ value detected in resolved transitions. An explanation must be sought in the structure properties of the Dy isotopes because a minimum of the fragmentation with respect to the neighboring isotones is also observed for the even-mass cases, and ^{164}Dy exhibits an unusually large $B(M1)$ strength because of spin strength admixtures. Microscopic calculations for odd-mass rare-earth nuclei are not yet capable to provide a realistic description of the experimental strength fragmentation, even for the most favorable case of ^{163}Dy. Thus, an interpretation is still missing.

ACKNOWLEDGMENTS

The support by the Deutsche Forschungsgemeinschaft under Contract Nos. Kn 154/30, Br 799/6-2, and FOR272/2-2 is gratefully acknowledged. J.E. acknowledges partial support through the U.S. National Science Foundation, Grant No. PHY-0110253.

[1] D. Bohle, A. Richter, W. Steffen, A.E.L. Dieperink, N. Lo Iudice, F. Palumbo, and O. Scholten, Phys. Lett. **137B**, 27 (1984).

[2] K. Heyde and A. Richter, Rev. Mod. Phys. (to be published).

[3] U. Kneissl, H.H. Pitz, and A. Zilges, Prog. Part. Nucl. Phys. **37**, 349 (1996).

[4] N. Lo Iudice and A. Richter, Phys. Lett. B **304**, 193 (1993).
[5] P. von Neumann-Cosel, J.N. Ginocchio, H. Bauer, and A. Richter, Phys. Rev. Lett. **75**, 4178 (1995).
[6] J. Enders, H. Kaiser, P. von Neumann-Cosel, C. Rangacharyulu, and A. Richter, Phys. Rev. C **59**, R1851 (1999).
[7] N. Pietralla, P. von Brentano, R.-D. Herzberg, U. Kneissl, N. Lo Iudice, H. Maser, H.H. Pitz, and A. Zilges, Phys. Rev. C **58**, 184 (1998).
[8] D. Zawischa, J. Phys. G **24**, 683 (1998).
[9] N. Lo Iudice, Riv. Nuovo Cimento **23**, 1 (2000).
[10] I. Bauske, J.M. Arias, P. von Brentano, A. Frank, H. Friedrichs, R.D. Heil, R.-D. Herzberg, F. Hoyler, P. Van Isacker, U. Kneissl, J. Margraf, H.H. Pitz, C. Wesselborg, and A. Zilges, Phys. Rev. Lett. **71**, 975 (1993).
[11] C. Schlegel, P. von Neumann-Cosel, A. Richter, and P. Van Isacker, Phys. Lett. B **375**, 21 (1996).
[12] J. Enders, N. Huxel, P. von Neumann-Cosel, and A. Richter, Phys. Rev. Lett. **79**, 2010 (1997).
[13] J. Enders, N. Huxel, U. Kneissl, P. von Neumann-Cosel, H.H. Pitz, and A. Richter, Phys. Rev. C **57**, 996 (1998).
[14] N. Huxel, P. von Brentano, J. Eberth, J. Enders, R.-D. Herzberg, P. von Neumann-Cosel, N. Nicolay, N. Pietralla, H. Prade, C. Rangacharyulu, J. Reif, A. Richter, C. Schlegel, R. Schwengner, S. Skoda, H.G. Thomas, I. Wiedenhöver, G. Winter, and A. Zilges, Nucl. Phys. **A645**, 239 (1999).
[15] J. Enders, T. Guhr, N. Huxel, P. von Neumann-Cosel, C. Rangacharyulu, and A. Richter, Phys. Lett. B **486**, 273 (2000).
[16] U.E.P. Berg and U. Kneissl, Annu. Rev. Nucl. Part. Sci. **37**, 33 (1987).
[17] G. Alaga, K. Alder, A. Bohr, and B.R. Mottelson, K. Dan. Vidensk. Selsk. Mat. Fys. Medd. **29**, 1 (1955).
[18] J. Margraf, T. Eckert, M. Rittner, I. Bauske, O. Beck, U. Kneissl, H. Maser, H.H. Pitz, A. Schiller, P. von Brentano, R. Fischer, R.-D. Herzberg, N. Pietralla, A. Zilges, and H. Friedrichs, Phys. Rev. C **52**, 2429 (1995).
[19] A. Nord, A. Schiller, T. Eckert, O. Beck, J. Besserer, P. von Brentano, R. Fischer, R.-D. Herzberg, D. Jäger, U. Kneissl, J. Margraf, H. Maser, N. Pietralla, H.H. Pitz, M. Rittner, and A. Zilges, Phys. Rev. C **54**, 2287 (1996).
[20] N. Pietralla, I. Bauske, O. Beck, P. von Brentano, W. Geiger, R.-D. Herzberg, U. Kneissl, J. Margraf, H. Maser, H.H. Pitz, and A. Zilges, Phys. Rev. C **51**, 1021 (1995).
[21] A. Müller, diploma thesis, Universität Stuttgart, 1997.
[22] H. Maser, S. Lindenstruth, I. Bauske, O. Beck, P. von Brentano, T. Eckert, H. Friedrichs, R.D. Heil, R.-D. Herzberg, A. Jung, U. Kneissl, J. Margraf, N. Pietralla, H.H. Pitz, C. Wesselborg, and A. Zilges, Phys. Rev. C **53**, 2749 (1996).
[23] C. Wesselborg, P. von Brentano, K.O. Zell, R.D. Heil, H.H. Pitz, U.E.P. Berg, U. Kneissl, S. Lindenstruth, U. Seemann, and R. Stock, Phys. Lett. B **207**, 22 (1988).
[24] N. Huxel, W. Ahner, H. Diesener, P. von Neumann-Cosel, C. Rangacharyulu, A. Richter, C. Spieler, W. Ziegler, C. De Coster, and K. Heyde, Nucl. Phys. **A539**, 478 (1992).
[25] J. Eberth, Prog. Part. Nucl. Phys. **38**, 495 (1992).
[26] V.G. Soloviev, A.V. Sushkov, N.Y. Shirikova, and N. Lo Iudice, Nucl. Phys. **A613**, 45 (1997).
[27] Y.D. Devi and V.K.B. Kota, Nucl. Phys. **A600**, 20 (1996).
[28] W. Ziegler, N. Huxel, P. von Neumann-Cosel, C. Rangacharyulu, A. Richter, C. Spieler, C. De Coster, and K. Heyde, Nucl. Phys. **A564**, 366 (1993).
[29] H.H. Pitz, U.E.P. Berg, R.D. Heil, U. Kneissl, R. Stock, C. Wesselborg, and P. von Brentano, Nucl. Phys. **A492**, 411 (1989).
[30] H. Friedrichs, B. Schlitt, J. Margraf, S. Lindenstruth, C. Wesselborg, R.D. Heil, H.H. Pitz, U. Kneissl, P. von Brentano, R.-D. Herzberg, A. Zilges, D. Häger, G. Müller, and M. Schumacher, Phys. Rev. C **45**, R892 (1992).
[31] A. Nord, Ph.D. thesis, Universität Stuttgart, 2000.
[32] W. Ziegler, C. Rangacharyulu, A. Richter, and C. Spieler, Phys. Rev. Lett. **65**, 2515 (1990).
[33] J. Margraf, R.D. Heil, U. Maier, U. Kneissl, H.H. Pitz, H. Friedrichs, S. Lindenstruth, B. Schlitt, C. Wesselborg, P. von Brentano, R.-D. Herzberg, and A. Zilges, Phys. Rev. C **47**, 1474 (1993).
[34] J.N. Ginocchio and A. Leviatan, Phys. Rev. Lett. **79**, 813 (1997).
[35] D. Bohle, G. Kilgus, A. Richter, C.W. de Jager, and H. de Vries, Phys. Lett. B **195**, 326 (1987).
[36] P.G. Hansen, B. Jonson, and A. Richter, Nucl. Phys. **A518**, 13 (1990).
[37] P. von Neumann-Cosel, F. Neumeyer, S. Nishizaki, V.Yu. Ponomarev, C. Rangacharyulu, B. Reitz, A. Richter, G. Schrieder, D.I. Sober, T. Waindzoch, and J. Wambach, Phys. Rev. Lett. **82**, 1105 (1999).
[38] A. Gilbert and A.G.W. Cameron, Can. J. Phys. **43**, 1446 (1965).
[39] W. Dilg, W. Schantl, H. Vonach, and M. Uhl, Nucl. Phys. **A217**, 269 (1973).
[40] P. Demetriou and S. Goriely, Nucl. Phys. **A695**, 95 (2001).
[41] T. von Egidy, H.H. Schmidt, and A.N. Behkami, Nucl. Phys. **A481**, 189 (1988).
[42] Y. Alhassid, G.F. Bertsch, S. Liu, and H. Nakada, Phys. Rev. Lett. **84**, 4313 (2000).
[43] N. Pietralla, Ph.D. thesis, Universität zu Köln, 1996.
[44] A. Linnemann, P. von Brentano, J. Eberth, J. Enders, A. Fitzler, C. Fransen, E. Guliyev, R.-D. Herzberg, L. Käubler, A. A. Kuliev, P. von Neumann-Cosel, N. Pietralla, H. Prade, A. Richter, R. Schwengner, H.G. Thomas, P. Weisshaar, and I. Wiedenhöver, Phys. Lett. B **554**, 15 (2003).
[45] P. von Brentano, J. Eberth, J. Enders, L. Esser, R.-D. Herzberg, N. Huxel, H. Meise, P. von Neumann-Cosel, N. Nicolay, N. Pietralla, H. Prade, J. Reif, A. Richter, C. Schlegel, R. Schwengner, S. Skoda, H.G. Thomas, I. Wiedenhöver, G. Winter, and A. Zilges, Phys. Rev. Lett. **76**, 2029 (1996).